Engineering Structures 136 (2017) 36–53

Contents lists available at ScienceDirect

Engineering Structures

journal homepage: www.elsevier.com/locate/engstruct

Fragility assessment of a RC structure under tsunami actions via nonlinear static and dynamic analyses

Crescenzo Petrone [a,*], Tiziana Rossetto [a], Katsuichiro Goda [b]

[a] Department of Civil, Environmental & Geomatic Engineering, University College London, London, United Kingdom
[b] Department of Civil Engineering, University of Bristol, University Walk, Bristol, United Kingdom

ARTICLE INFO

Article history:
Received 14 April 2016
Revised 3 January 2017
Accepted 5 January 2017

Keywords:
Tsunami engineering
Fragility curve
Analysis methodology
Pushover analysis
Time-history analysis
Tsunami force
Tsunami simulation

ABSTRACT

Current guidelines for design and assessment of buildings under tsunami actions do not explicitly state how to apply tsunami loads to buildings and which analysis methods to use in order to assess the structural response to the tsunami loads. In this paper, a reinforced concrete (RC) moment-resisting frame, which is designed as a tsunami evacuation building, is selected as a case study and subjected to simulated 2011 Tohoku tsunami waves. To assess tsunami impact on the model building, different nonlinear static analyses, i.e. constant-height pushover (CHPO) and variable-height pushover (VHPO), are compared with nonlinear dynamic analysis. The results of VHPO provide a good prediction of engineering demand parameters and collapse fragility curves obtained from the dynamic analysis under a wide range of tsunami loading. On the other hand, CHPO tends to overestimate interstorey drift ratio (IDR) and underestimate column shear by about 5–20%. It provides a larger fragility, i.e. about 10% in median value, for global failure and a smaller fragility for local shear failure. On the basis of these results, it is recommended that VHPO be used in future fragility analysis of buildings subjected to tsunami. However, pushover methods might not be adequate in cases where the tsunami inundation force time-histories are characterised by a "double-peak", which subjects the structure to a two-cycle load. Finally, it is found that tsunami peak force is better correlated to IDR than flow velocity and inundation depth for the considered structure. This suggests that the peak force would be a more efficient intensity measure than the other two in the development of tsunami fragility curves.

1. Introduction

Recent tsunami events (e.g. 2004 Indian Ocean tsunami and 2011 Great East Japan tsunami) have caused numerous deaths and widespread damage. The 2004 Indian Ocean tsunami caused 230,000 deaths [1], whereas the 2011 Great East Japan (Tohoku) earthquake-tsunami caused 19,000 fatalities as well as US$211 billion direct economic loss [2]. It is worth noting that such a loss does not include costs related to the Fukushima Daiichi nuclear power plant crisis nor indirect losses, such as supply-chain disruptions and retail trade and tourism reduction due to restrained consumption and radiation fears.

These observed consequences from tsunami can only be reduced through the development of comprehensive risk mitigation plans based on tsunami impact scenarios and risk assessments. An important component in the evaluation of tsunami risk is the estimation of building fragility due to tsunami onshore flow. This has recently been recognised by researchers worldwide [3–5]. To date the majority of this research has focussed on the development of fragility functions based on observational post-tsunami damage data, in particular after the 2004 Indian Ocean tsunami (e.g. [6,7]) and the 2011 Japan tsunami (e.g.[3]). Empirical tsunami fragility functions are by their nature specific to the event represented in the post-event damage data as well as the local building stock, and suffer from absence of locally recorded tsunami intensity measures (IMs). Tsunami inundation depths can be obtained from the inspection of water marks on standing buildings, whereas other IMs, such as flow velocity, are difficult to assess after the event. It is important to recognise that the building damage observation data have been affected by both earthquake and tsunami loads, and implicitly include the response of buildings to the combined hazards. As post-tsunami reconnaissance cannot distinguish damage due to the two hazards, it is difficult to determine whether the preceding damage due to the earthquake has affected the structural response to the tsunami inundation. The assessment of structural performance through numerical analyses is therefore

* Corresponding author.
E-mail addresses: c.petrone@ucl.ac.uk (C. Petrone), t.rossetto@ucl.ac.uk (T. Rossetto), Katsu.Goda@bristol.ac.uk (K. Goda).

http://dx.doi.org/10.1016/j.engstruct.2017.01.013
0141-0296/

essential to overcome the mentioned limitations of empirical fragility functions. Analytical fragility functions can also be used together with empirical assessments to provide a deeper understanding of structural behaviour under tsunami actions.

1.1. Previous studies on analytical fragility functions and structural assessment to tsunamis

Very few studies concerning analytical fragility of structures to tsunami are available in the literature. Macabuag et al. [8] presented a preliminary study where they considered different building codes in assessing the tsunami force on a simple reinforced concrete (RC) frame building based on a pushover-based method. investigated the behaviour of RC buildings under tsunami loads by means of both experimental and numerical analyses and assessed the contribution of infill walls on the response of the structure. A set of tsunami pushover curves for a single-storey RC structure was produced assuming a constant inundation height. It was found that shear failure in columns leads the structure to failure before the full structural capacity is exploited. Nanayakkara and Dias [9] proposed analytical fragility curves for different structural typologies. A probabilistic model based on Monte Carlo simulation was used to artificially produce fragility curves for simplified masonry and RC structural models assuming that inundation depth is uniformly distributed for different inundation depth ranges. A good match with empirical fragility curves was observed. In addition, preliminary studies on the behaviour of structures under ground motion and subsequent tsunami inundation are available in the literature. For instance, Park et al. [10] proposed an approach to consider the successive seismic and tsunami risk to buildings. The structure was modelled as an equivalent single-degree-of-freedom system and was subjected first to an acceleration time-history and then a tsunami force calculated from FEMA P646 [11]. Latcharote and Kai [12] implemented a sequential earthquake and tsunami simulation in an Integrated Earthquake Simulation to assess the expected damage for a three-storey RC structure in Kochi, Japan.

All these existing tsunami analytical fragility approaches are associated with a number of issues that affect their accuracy. Firstly, the tsunami action is typically modelled with an equivalent force according to design prescriptions, without taking into account realistic tsunami inundation time-histories. Current design building codes might be inadequate in assessing tsunami force; in particular, conservative assumptions are typically made for design purposes. Secondly, gross assumptions are made regarding the pressure distribution along the height of the structure resulting from the tsunami actions, without consideration of the potential sensitivity of the structural response to variations in the pressure distribution or how the load is discretised and applied to the structural model. Furthermore, almost none of the approaches consider the fact that tsunami forces are applied at the rear of the structure as the tsunami wave flows past the building. Thirdly, available studies typically consider only nonlinear static analyses pushing the structure up to the structural peak strength, where the structure cannot be considered to have failed. It is clear that there is a gap in knowledge in determining how tsunami loads should be applied to a building and which analysis methodology is most suitable for the estimation of building response to realistic tsunami.

1.2. Objectives of the study

This paper takes a first step to address the above mentioned issues by assessing different nonlinear static analyses and comparing them with dynamic analyses performed considering realistic tsunami inundation time-histories. The assessment is performed in terms of the ability of each nonlinear static method to predict the peak structural response observed in the dynamic analyses and to reproduce the tsunami fragility curves developed from the dynamic analyses. The peak structural response, e.g. maximum interstorey drift ratio (IDR), is referred to as "demand" in the following, whereas the tsunami peak intensity is expressed in terms of IM, e.g. inundation depth. The study takes advantages of the numerical-experimental studies developed at UCL and HR Wallingford for the assessment of tsunami forces on structures [13,14] and the extensive tsunami simulations for generating realistic tsunami wave traces [15]. The paper is divided into different sections. First, a case study building, a Japanese tsunami evacuation building, is described and then its modelling is discussed. Particular attention is paid to the definition of tsunami load through the adoption and modification of the formulation of Qi et al. [13]. A tsunami inundation simulation of the 2011 Tohoku tsunami is presented in order to define numerous tsunami wave traces in terms of inundation depth and flow velocity, for use in the dynamic analyses of the structural model. Different non-linear static analysis methodologies for the assessment of the building response are defined and a sensitivity analysis is performed to assess the influence of applied load distribution on the structural response under tsunami actions. The demand on the building, in terms of maximum IDR and shear, is then evaluated using the defined nonlinear static analysis methods and compared to the results of the nonlinear dynamic analysis, with the aim of identifying the bias induced by adopting the former simpler analyses. Such a bias is finally estimated in terms of tsunami fragility curve, and recommendations are made as to which nonlinear static analysis and load distribution approach are the most suitable for use in the study of building fragility to tsunami. It is highlighted that the fragility functions presented in this paper are specific to the case study building and should not be adopted in the assessment of other RC building types.

2. Methodology

2.1. Case study building

The case study building selected is an ideal tsunami evacuation building, consisting of 10 storeys and RC frames in both horizontal directions (Fig. 1). Building plan dimensions are 36×23 m, with a constant 3.9 m interstorey height for all storeys except for the ground storey, which is 4.5 m high. Six and three bays can be identified along the longitudinal and transverse directions, respectively. The tsunami evacuation building is taken from the design example 3-1 of the "structural design and members section case studies" [16]. This structure is an ideal tsunami evacuation building, designed according to both earthquake and tsunami actions. It should not be considered as representative of a typical mid-rise RC building in Japan, e.g. the apartment building in Rikuzentakada [17] and other RC frame buildings that were surveyed after the 2011 Japan tsunami [18–20]. The example structure is designed assuming an earthquake zone coefficient $Z = 1.0$, soil type 2, fundamental vibration period 0.796 s, characteristic vibration coefficient $Rt = 0.979$ and base shear coefficient $C_0 = 0.2$. The structure is also designed to resist tsunami loads, assuming a 10 m inundation depth and coefficient a equal to 2.0, yielding an effective inundation depth equal to 20 m in calculating the wave forces action the building. Only minor modifications from the seismic design result are made for the tsunami design of the structure, particularly concerning the building foundations. However, the tsunami design is conducted assuming that the first two floors are "pilotis", i.e. do not have infills. This study neglects the presence of openings; it is assumed that water flow is obstructed in all bays for the whole height of the structure. Such an assumption

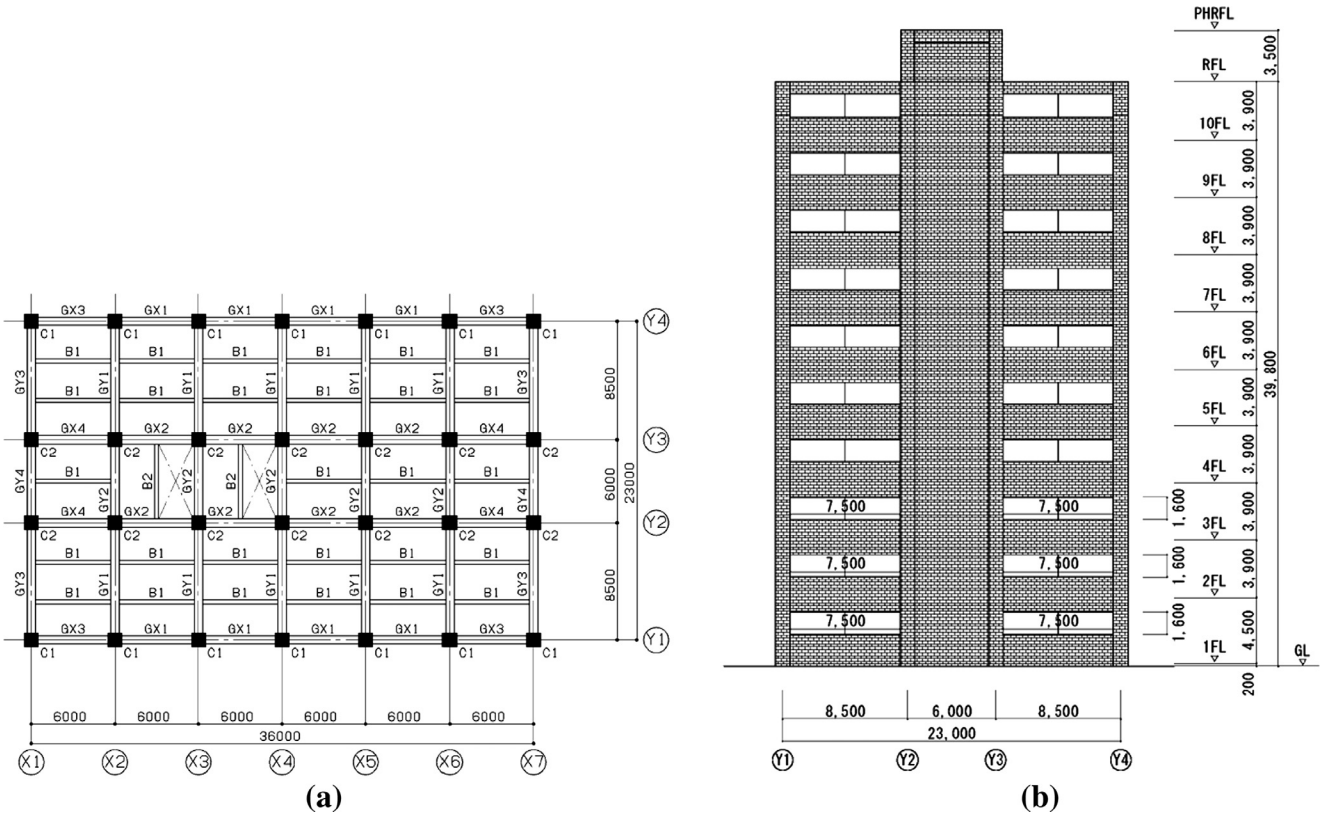

Fig. 1. Case study structure: (a) plan view and (b) lateral view [16].

results in an increase in tsunami force and allows the investigation of a more common case, where infill walls are installed throughout the height of the structure.

Different concrete classes are employed in the design of the structure, with decreasing concrete strength adopted along its height; an Fc40 class is employed for the first three storeys, Fc36 for the fourth and fifth storeys, Fc30 for the sixth and seventh storeys, and Fc27 for the upper three storeys. It should be noted that Fc40 has the characteristic strength of 40 N/mm^2. Two different steel typologies are used: (a) SD390, having the characteristic strength of 390 N/mm^2, for longitudinal reinforcement and (b) SD295 for transversal reinforcement.

Column cross-sections assume constant dimensions throughout the building, i.e. 100 × 100 cm. They are reinforced with a longitudinal reinforcement ratio ranging from 1.32% to 2.25%. The stirrups have a diameter of 13 mm with a 100 mm spacing; at lower storeys additional ties are also provided in order to increase both shear strength and concrete confinement. Beam cross-section dimensions range from 60 × 100 cm (at the first floor) to 40 × 85 cm (at the top floor). Longitudinal reinforcement in beams also varies along the building height, ranging from eight 32 mm-diameter bars at top and bottom flanges (at the first storey) to three 25 mm-diameter bars (at the top floor). 13 mm-diameter stirrups are also adopted in the beams with a spacing ranging from 100 mm to 200 mm.

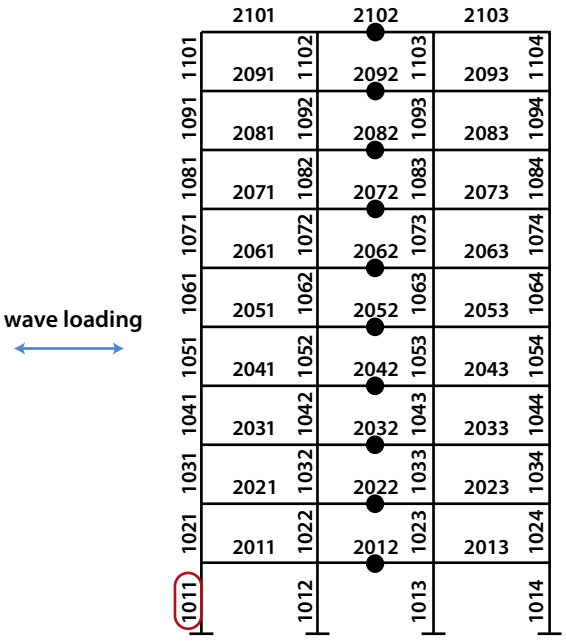

Fig. 2. Geometric configuration of the considered RC frame structure.

2.2. Structural modelling

The case study building is modelled within an OpenSees platform [21]. A 2D model of a transversal frame of the structure is considered (Fig. 2); its behaviour is assumed to be representative of the whole structure since all transverse frames are identical. One seventh of the seismic mass of the corresponding 3D building is assigned to a master joint at each floor.

A distributed plasticity approach is adopted for the RC frame model. Each element is modelled with a force-based nonlinear beam-column element, assuming five integration points. Cross-sections are modelled by means of a fibre approach. Three different constitutive laws are defined to model column cross-sections: (a) unconfined concrete is associated with cover fibres; (b) confined concrete is associated with core fibres; and (c) steel material is linked to steel discrete fibres. The stress–strain relationship

proposed by [22], i.e. *Concrete04* in OpenSees, is selected for both unconfined and confined concrete, whereas a bilinear stress-strain envelope with a smooth transition from elastic to plastic branches, i.e. *Steel02* in OpenSees, is adopted for steel. Mean strengths of steel and unconfined material are assessed assuming the coefficient of variation of 5% and 10% for steel and concrete, respectively [23]. The ultimate steel strain is set equal to 30% and the ratio between tensile strength and yielding strength is set equal to 1.50 [23]. A 5 cm cover is assumed for all cross-sections. It should also be noted that unconfined concrete is adopted for core fibres in beams, due to the absence of axial force and the consequent limited confinement effect. Mass values are assessed considering a mass per unit area equal to 1.2 t/m^2 and consistent gravity loads are applied to the beams. The structural model exhibits a fundamental vibration period of 0.73 s.

2.3. Tsunami load assessment

The tsunami action on the structure is estimated with an equivalent force approach, as suggested in current design guidelines for tsunami resistant structures, e.g. [11], and is modelled through a lateral force, which is caused by the fluid-structure interaction. An existing experimental-analytical research study by [13] is employed for this purpose. The study assessed the drag force acting on a rectangular building placed in a free-surface channel flow; the formulation was experimentally validated. Qi et al. [13] demonstrated that two different flow regimes can occur for a given inlet steady-state flow impacting an obstacle: subcritical and choked. The transition between the two regimes is determined by the Froude number of the impacting flow. As the Froude number increases, a hydraulic jump downstream of the obstacle is observed and the flow condition turns from subcritical into choked. It was found that the blocking ratio, i.e. the ratio between building width b and flume width w, influences the Froude number threshold between the two regimes. According to Qi et al. [13], the tsunami force per unit structural width can be estimated as follows:

$$F/b = sgn(u)\begin{cases} 0.5C_D\rho u^2 h & \text{if } Fr < Fr_c \\ \lambda\rho g^{1/3}u^{4/3}h^{4/3} & \text{if } Fr \geqslant Fr_c \end{cases} \quad (1)$$

where $sgn(u)$ is the sign function of the flow velocity, C_D is a drag coefficient, ρ is the density of the fluid assumed 1.20 t/m^3, u is the flow velocity, h. the inundation depth, λ is the leading coefficient, g is the acceleration of gravity, and $Fr = u/\sqrt{g \cdot h}$ is the Froude number. It should be noted that the force formulation for the subcritical condition *resembles* the hydrodynamic component of the tsunami force included in FEMA P646 [11]. The Froude number threshold Fr_c is estimated from the following equation [13]:

$$\left(1-\frac{C_H b}{w}\right)\frac{1}{2Fr_c^{4/3}}+\left(1-\frac{C_D b}{2w}\right)Fr_c^{2/3}=\left(1-\frac{C_H b}{w}\right)\frac{1}{2Fr_{d,c}^{4/3}}+Fr_{d,c}^{2/3};$$
$$Fr_{d,c}=\left(1-\frac{C_H b}{w}\right)^{1/2} \quad (2)$$

where C_H is experimentally calibrated to the value of 0.58 and $Fr_{d,c}$ is the Froude number at the back of the building in a critical condition, i.e. when the flow turns into choked. The drag and leading coefficients are a function of the blocking ratio b/w and can be estimated as [13]:

$$C_D = C_{D0}\left(1+\frac{C_{D0}b}{2w}\right)^2;$$
$$\lambda = \frac{1}{2}C_D Fr_c^{2/3}+\frac{1}{2}C_H\left(\frac{1}{Fr_c^{2/3}}-\frac{1}{Fr_{dc}^{4/3}}\right) \quad (3)$$

where C_{D0} is equal to 1.9.

It is assumed that the steady-state flow force formulation can be applied to the case of tsunami inundation. Tsunami flows are unsteady; however, they can be considered quasi-steady when due to their extremely long wavelengths, the temporal variation of the flow is small, especially with respect to the length scale of a building. Two different blocking ratios are assumed in this study, in order to be representative of a dense ($b/w = 0.6$) and sparse ($b/w = 0.1$) built environment (Table 1).

The tsunami force F is evaluated assuming a 6 m influence width b, equal to the spacing among transversal frames (Fig. 1). The above mentioned formulation allows estimating the tsunami force from two input parameters: flow velocity and inundation depth. For a given tsunami inundation flow time-history, the formulation can be applied at each time step in order to assess tsunami force time-history. To avoid discontinuities in force time-histories as the flow state goes from subcritical to choked and vice versa, a smoothing function is applied to the $C_D - Fr$ function (Fig. 3). A cubic smoothing function is applied from the Froude number $\overline{Fr}$, which is characterised by $Fr_d = 1.2\overline{Fr}$, to Fr_c; the drag coefficient varies from the value assessed with Eq. (3) to the value $C_{D,choked}$ required to equal subcritical and choked forces at Fr_c. From Eq. (1), it can be demonstrated that $C_{D,choked} = 2\lambda Fr_c$.

Qi et al. [13] focused on the assessment of net flow force. However, there is no indication about how the force calculated should be distributed along the height of the building as well as between the front and the back of the building. Recent studies s uggest that the pressure distribution due to tsunami flow is linear [24]. As the slope of such a pressure distribution is unknown, it is decided to (a) apply only net force in front of the structure and (b) consider two different load patterns representative of extreme cases (Fig. 4a):

- A triangular load pattern, which assumes that pressure distributions at the front and at the back are characterised by different slopes with the same water depth
- A trapezoidal load pattern, which assumes that pressure distributions at the front and at the back are characterised by the same slope with different water depths.

Pressure distributions are then characterised by the following p_d value:

$$p_d = \frac{2F}{h_1 + h_d} \text{ for trapezoidal loads} \quad (4)$$

$$p_d = \frac{2F}{h_1} \text{ for triangular loads} \quad (5)$$

Inundation depth at the back of the structure h_d can be estimated from Fr_d (Fig. 3) by assuming that the volume flux is conserved from the front to the back of the building (Fig. 4b).

In summary, it is important to recall the assumptions adopted in this study for the assessment of tsunami force from a given tsunami wave trace.

- The formulation developed by [13] for steady-state flow is assumed to be valid also in unsteady-state conditions and for the Froude numbers larger than Fr_c.
- Only net force is applied at the front of the building. Future experimental and numerical studies will consider two different load patterns at the front and at the back of the structure. It should be noted that this assumption would not cause any bias on the assessment of the global performance of the building, whereas the local demand (e.g. shear demand in columns) might be biased.

Table 1
Tsunami load parameters for two different blocking ratios.

b/w	C_D	λ	Fr_c
0.1	2.3	1.1	0.68
0.6	4.7	2.0	0.32

- Several additional effects due to tsunami, which might significantly influence the fragility assessment, are not considered in this study, such as debris impact, buoyancy, and scour of foundation. Specific studies will be focused on these important topics, which might have a significant influence on the fragility assessment.

2.4. Tsunami wave simulation

Tsunami wave simulation is required in order to assess the impact on the case study structure due to a realistic tsunami. The study by [15] generated numerous tsunami wave traces for the 2011 Tohoku tsunami. Tsunami inundation is estimated in terms of inundation depth and flow velocity by evaluating nonlinear shallow water equations with run-up [25]. The information on bathymetry, surface roughness, and coastal defence structures is obtained from the Miyagi prefectural government, Japan Hydrographic Association and Geospatial Information Authority of Japan. The bottom friction is evaluated using Manning's formula. Computational cells include those on land, and coastal defence structures are taken into account using an overflowing formula. The initial water displacement caused by earthquake rupture is assessed according to [26] and [27]. Tsunami simulations are performed considering four nested domains (1350-m – 450-m – 150-m – 50-m) and wave-propagation duration of 2 h with a 0.5 s integration time step. It should be acknowledged that simulated tsunami wave traces can be affected by the selected mesh resolution, i.e. 50 m in this study, the roughness and the Digital Elevation Model quality. In particular, the simulations could be performed using a very fine mesh, up to a 5 m (or 10 m) resolution [28–30]. To investigate the effects of mesh resolution, sensitivity analyses are performed that compare the simulated tsunami wave height and flow velocity time-histories along the coastal line of Miyagi Prefecture for 50 m and 10 m mesh data. The results indicate that the effects of mesh resolution are not significant for the tested locations. Based on these results the 50 m resolution is adopted to reduce computational effort.

Tsunami simulation is performed considering different slip distributions along the fault: the slip distribution by Satake et al. [31], which was inferred from tsunami waveform data, as well as ten different stochastic realisations of such a slip distribution included in [15]. Peak inundation depth and flow velocity can be estimated over a wide region, whereas their time-histories are recorded at specific locations. In this study, 73 different locations along the Tohoku coastline are considered for the 11 adopted slip distributions, yielding 803 different tsunami wave traces. The selection of the locations takes into account different coastal conditions, (e.g. plain- vs ria-type), and particularly focuses on the regions where large inundation depths occurred. The wave traces simulated according to the slip distribution by Satake et al. [31] (Fig. 5) exhibit a good agreement with the observed peak inundation depth (i.e. about 10 m) and flow velocity (i.e. between 3 and 5 m/s) for several locations in the Kesennuma Bay area [32,33]. A similar conclusion can be drawn for a location close to Natori river at 2.5 km from the shoreline, where simulated peak velocity is about 3 m/s as observed by Hayashi and Koshimura [34].

Tsunami force can be estimated for each tsunami inundation time-history, according to the process shown in Fig. 6. It is assumed that the structural longitudinal direction is oriented along the North-South (NS) direction. Hence, flow velocity in the East-West (EW) direction is considered in the force assessment. The Froude number is evaluated for each time step to define whether the flow is subcritical or choked, and the corresponding formulation is employed to assess tsunami force. The Froude number thresholds for $b/w = 0.1$ and $b/w = 0.6$ are highlighted with dotted lines in Fig. 6. In dynamic analysis, time-histories are considered up to the time step corresponding to a 20% inundation depth drop from its peak value, which typically corresponds to low force values. They are trimmed in order to reduce the computational effort. All tsunami force time-histories are grouped according to their peak inundation depth. It is noted that the peak force does not typically occur at the same time as the peak inundation depth. Note that many of the defined time-histories are discarded as they yield very low tsunami forces, i.e. smaller than 2000 kN, which would not cause any damage in the structure. Finally, 249 time-histories are used for the 0.6 blocking ratio and 125 for the 0.1 blocking ratio.

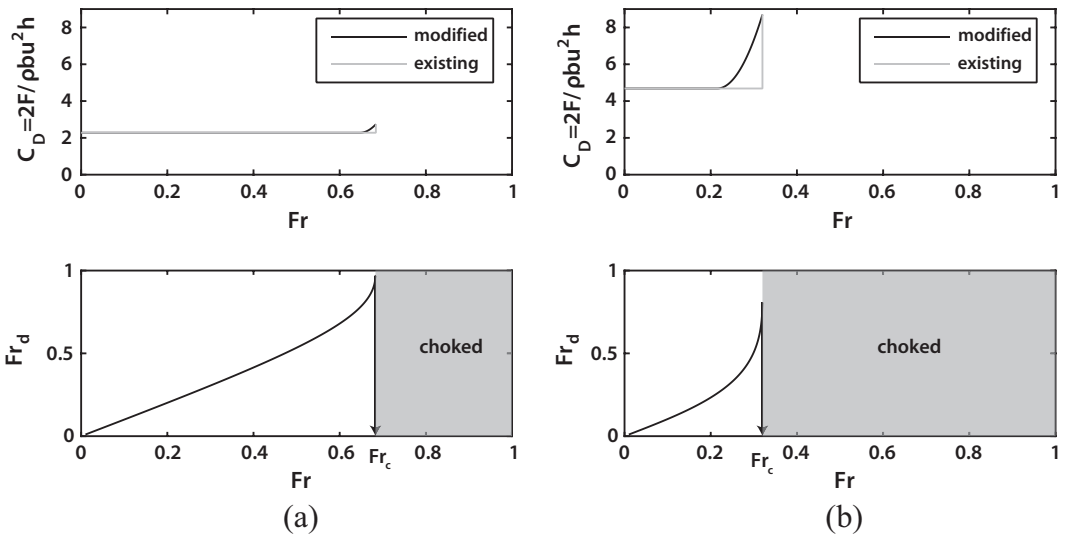

Fig. 3. Modification of drag coefficient in the vicinity of critical conditions for (a) $b/w = 0.1$ and (b) $b/w = 0.6$.

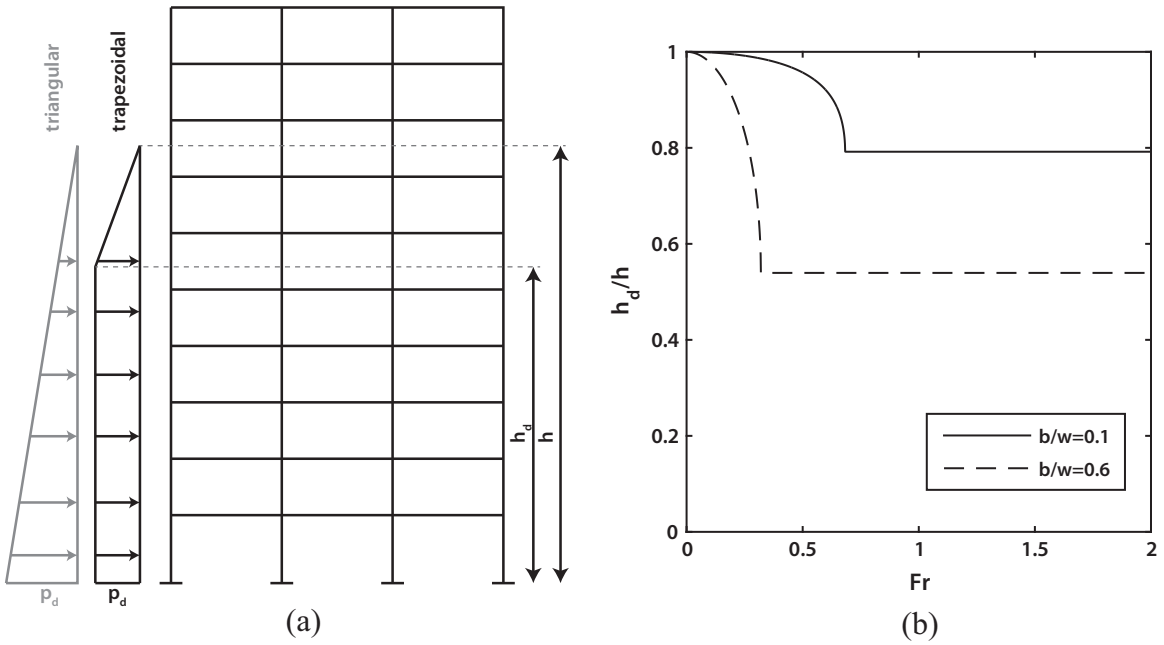

Fig. 4. (a) Pressure distributions of tsunami force. (b) Ratio between water height at the back of the structure and inundation water depth versus the Froude number.

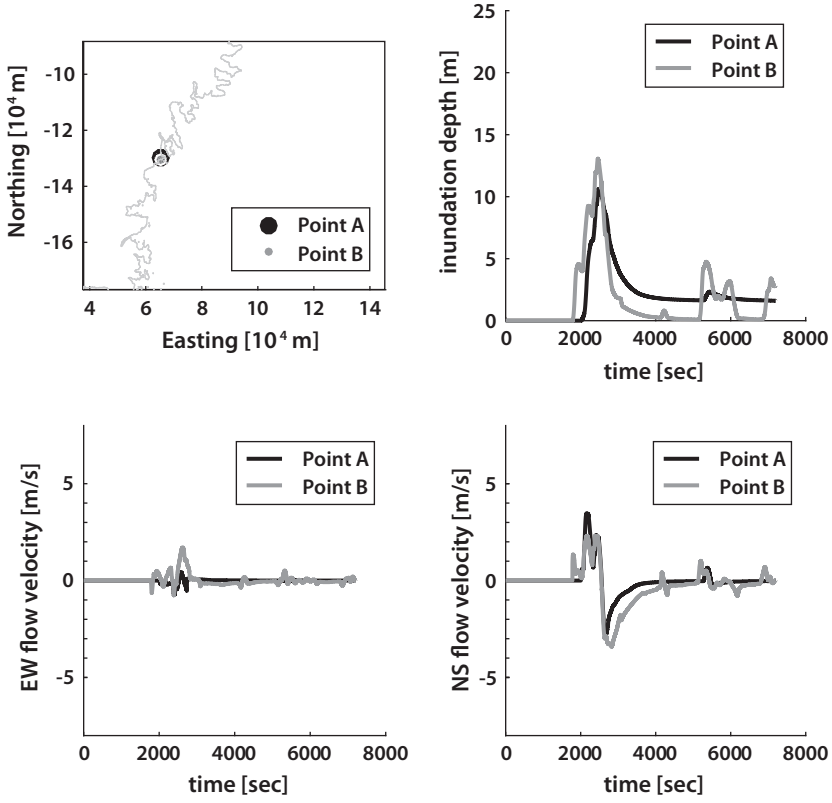

Fig. 5. Simulated wave traces in two different locations in Kesennuma Bay area.

2.5. Analysis methods

One of the main aims of the study is the assessment of the most reliable method to evaluate the structural performance under tsunami actions. Tsunami structural behaviour can be evaluated by adapting analysis approaches typically used in structural dynamics applications. Here, the case study structure is analysed by means of three different methodologies, features of which are summarised in Table 2:

- Time-history analysis considering actual tsunami onshore flow time-histories (TH).
- Nonlinear static analysis with constant-height load pattern (CHPO).

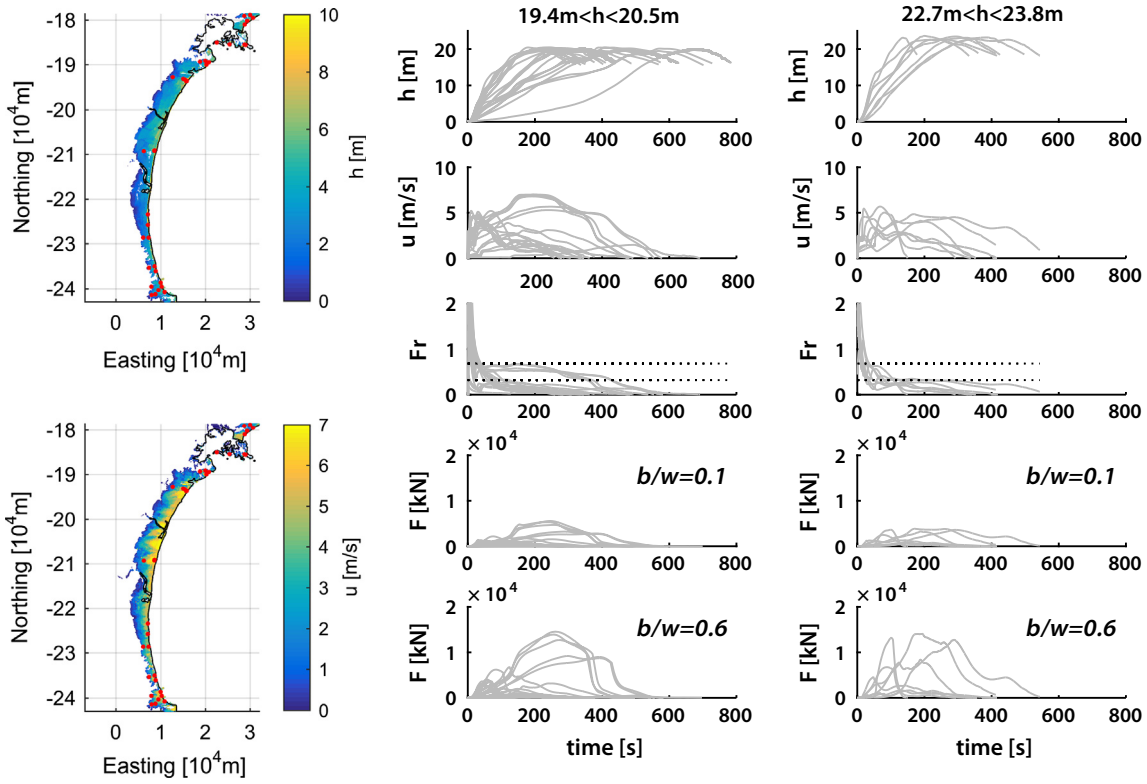

Fig. 6. Tsunami simulation results and tsunami load assessment. The two figures on the left denote the maximum inundation height h and flow velocity u, as well as some locations where tsunami traces are computed (red dots). The time histories on the right highlight the force assessment for tsunami wave traces corresponding to two different ranges of maximum inundation depth. (For interpretation of the references to colour in this figure legend, the reader is referred to the web version of this article.)

Table 2
Features of the considered analysis methodologies.

	CHPO	VHPO	TH
Inundation depth	Constant	Linearly increasing	Actual
Froude number	Increasing	Constant	Actual
Solver	Static	Static	Dynamic
Integrator	Displacement controlled	Force controlled	Newmark

- Nonlinear static analysis with variable-height load pattern (VHPO).

In TH, a dynamic time-history analysis is carried out considering the tsunami force estimated from the simulated time-histories of tsunami onshore flow according to the formulation presented in Section 2.3. The analysis allows the incorporation of the dynamic behaviour of the structure, a feature regarded to be important in the literature but never to date rigorously evaluated. Within this paper, the analysis used adopts a transient solver to allow for post-peak behaviour of the structure to be investigated. In particular, once the building's peak strength is reached, any increase of force is absorbed in terms of inertia force, which leads the structure to undergo large inelastic deformation. The transient solver is modified in order to capture the post-peak behaviour. To avoid convergence issues, the time step is reduced by a factor of 25.

Tsunami force is influenced by both inundation depth and flow velocity. Several pushover methods can be implemented to assess the response of the structure at a given target load (Fig. 7), assuming some constraints on these two IMs: by increasing the flow velocity and keeping inundation depth constant (CHPO), or by varying the depth and calculating the corresponding flow velocity assuming a constant Froude number (VHPO).

Nonlinear static analysis with the constant-height load pattern (CHPO) assumes a load pattern for a given inundation depth. Similarly to standard pushover analysis, this analysis method increases the roof displacement stepwise and evaluates the load magnitude required to attain pre-defined displacement demand levels (Fig. 7). This methodology is similar to earthquake pushover analysis [35], although it is characterised by a different load pattern (see Section 2.3). It can be interpreted as an analysis where a constant height load pattern is assumed with a variable flow velocity. This analysis be exploited to evaluate structural performance for a given flow velocity (or Froude number) and inundation depth. In particular, a performance point, characterised by the target force level corresponding to the assumed IMs, is identified on the pushover curve; such a point yields the predicted response of structure, e.g. interstorey drift demand.

Nonlinear static analysis with the variable-height load pattern (VHPO) considers a load pattern characterised by a variable height throughout the analysis (Fig. 7). At each analysis step, the load pattern height is modified according to the assumed inundation depth and the velocity is calculated by assuming a constant Froude number. It is preferred to keep the Froude number constant rather than the flow velocity since it is more realistic to assume that the Froude number is constant for a wide range of inundation depths, as also shown in typical tsunami onshore flow time-histories (Fig. 6). While CHPO is displacement-controlled, i.e. roof displacement is increased step-wise, VHPO is force-controlled. This feature might cause numerical convergence issues in VHPO as, for instance, the inability to capture any degrading branch in the pushover curve.

It should be highlighted that the existing literature typically considers CHPO to investigate the structural performance [36]

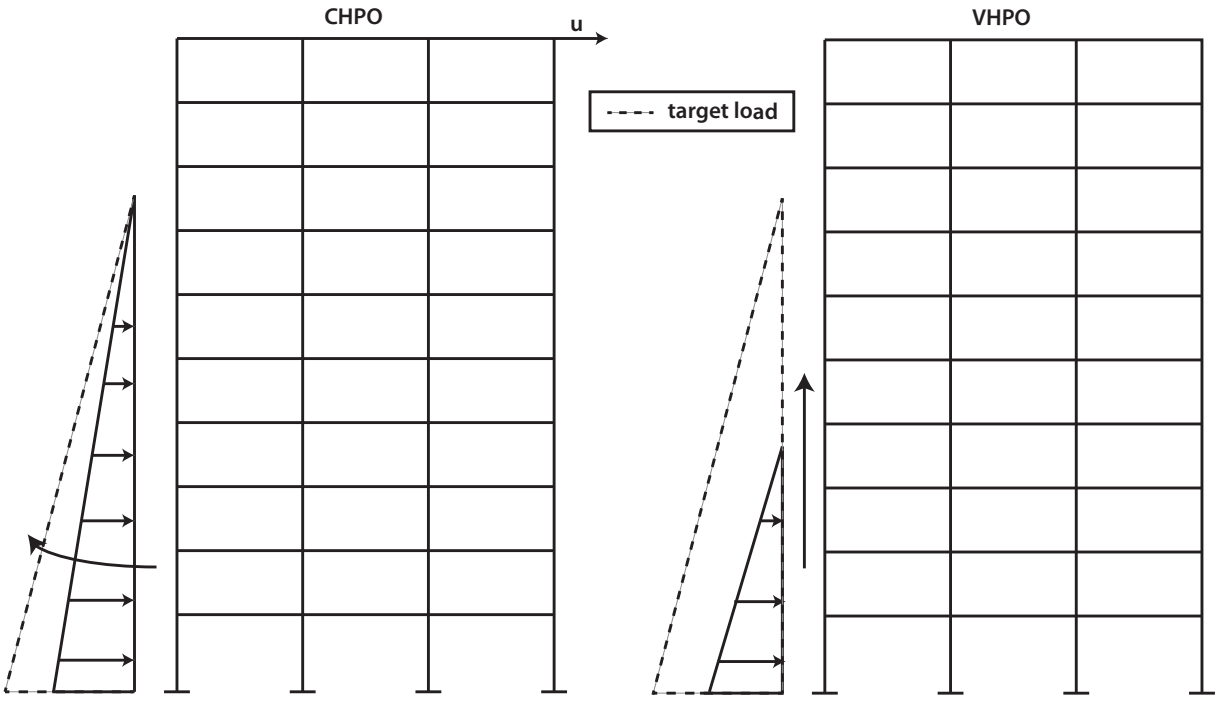

Fig. 7. Evolution of the load patterns in CHPO and VHPO for a given target load.

and that VHPO and TH are applied for the first time in this study. Future activities will focus on the identification of a pushover procedure which combines the two pushover methods presented herein in order to capture the post-peak behaviour and to adopt a realistic load pattern evolution.

2.6. Collapse identification

The main aim of the considered analysis methodologies is the assessment of the collapse damage state for a given tsunami input. Such a limit state may be attained for either a global failure or a local failure in the structure. Global failures typically refer to plastic mechanisms which involve a variable number of storeys and lead the structure to large displacements, whereas local failures may occur due to shear failure of a single element. Local failure is identified as the attainment of shear capacity in a member according to the formulation proposed by [37].

Different approaches are adopted to detect the global failure in the pushover analyses and the time-history analysis (Fig. 8). For the pushover analyses, the structure is assumed to be failed when the tsunami peak force exceeds the structural strength; the structural strength is assessed as the peak force in the pushover curve. This definition of collapse implicitly assumes that ductility does not play a role in the structural assessment. For the sake of clarity, Fig. 8a shows CHPO curves for a structure that had collapsed and not, under a predefined tsunami peak force.

For the time-history analysis, instead, the collapse is estimated from the outcomes of the analysis in two different ways. First, it is assumed that the collapse is attained if the structure is deformed up to a displacement which is characterised by a 20% internal force reduction (red point in Fig. 8b); such a reduction is in line with the failure detection dealing with structural elements [38]. It is worth noting the significant discrepancy between internal forces and the applied tsunami force in Fig. 8b after the peak force is reached. Such a discrepancy is equilibrated by the developed inertia and damping forces, which lead the structure to undergo large displacements and, hence, collapse. This collapse criterion is different from the one used to evaluate the collapse from the pushover analyses. Hence, the second collapse definition is adopted wherein the collapse occurs when the structure exhibits an IDR equal to a drift which occurs at the location of the structure peak strength in the pushover analysis (orange point in Fig. 8b). Such a collapse criterion is consistent with that defined for the pushover analysis.

3. Load discretisation sensitivity analysis

Design provisions [11] for structures under tsunami actions give clear indications as to how to assess the tsunami force distribution on the structure. However, they do not explicitly state how best to apply the tsunami loads to the building in structural analysis. The distributed tsunami load should be discretised into several point loads, since non-uniform distributed loads, e.g. trapezoidal loads, could not be applied to elements in many finite-element method programs, e.g. OpenSees [21]. Therefore, a load sensitivity analysis should be performed to assess how to apply tsunami loads to the structure. The results of the sensitivity analysis are illustrated here only for the 0.10 blocking ratio and the triangular load pattern. However, similar conclusions can be drawn when the blocking ratio of 0.60 or the trapezoidal load pattern is used. For the sensitivity analysis, four different load discretisation methods are considered (see Fig. 9).

- Load discretisation (A), where the tsunami load is discretised into n equally-spaced distributed loads; the point force resulting from each of the n distributed loads is assessed and applied to the structure at the centroid of distributed loads. This load discretisation is characterised by the same load magnitude and applied bending moment as the original distribution.
- Load discretisation (B) considers point loads applied at each storey; an influence area approach is adopted to assess the magnitude of each point load, with the distributed load acting among two consecutive mid-interstorey heights considered. This load discretisation results in a different load magnitude and applied bending moment from the original distribution.

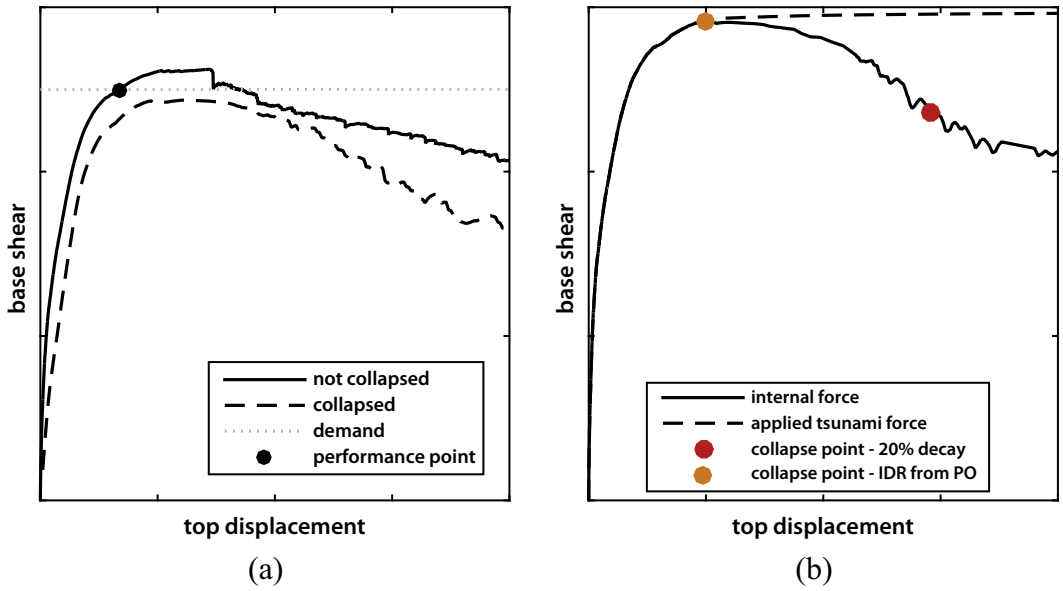

Fig. 8. Collapse identification in (a) pushover and (b) time-history analyses using a 20% strength reduction criterion.

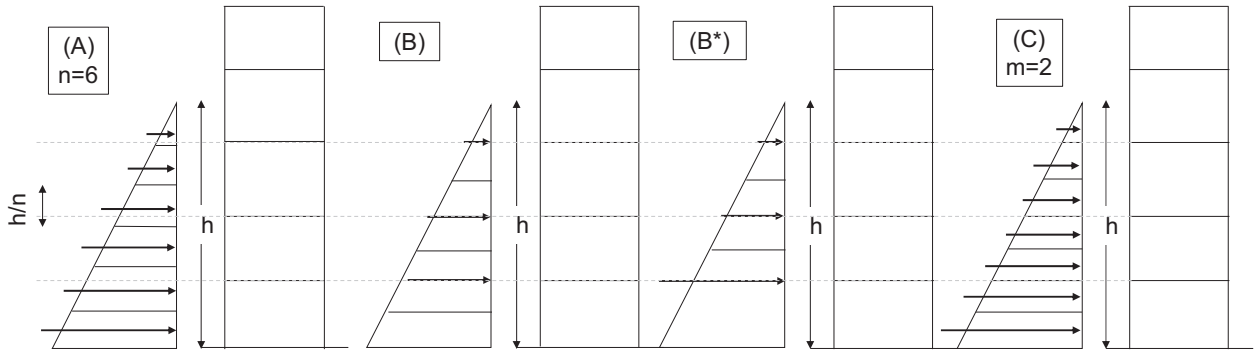

Fig. 9. Load discretisation methods for a given tsunami inundation depth.

- Load discretisation (B*) is the same as (B) except that in calculating the point load at the first storey it considers the full distributed force acting on the ground storey as contributing to the point load, instead of half.
- Load discretisation (C) assumes that the distributed force is discretised into *m* portions for each storey; a point force is applied to the structure at the centroid of each distribution. This approach is similar to (A), with the difference that (C) assumes an equal number of point loads for each storey. For this reason, the load discretisation (C) is preferred in analyses where the inundation depth is varied (i.e. VHPO and TH), since the load application locations can be approximately assumed constant throughout the analysis. In the case of (A) instead, the load application points vary significantly throughout the analysis.

The four load discretisation approaches are compared in terms of both global and local demands by means of several CHPO analyses. Different tsunami inundation depths are considered in order to investigate a wide range of structural responses. The values of *n* and *m* are also varied in the cases of (A) and (C), respectively, with *n* and *m* taking values of 5, 10 and 20, and 2, 3 and 5, respectively. These load cases are compared to a reference load discretisation, i.e. load discretisation (A) with *n* equal to 100.

Pushover curves are plotted up to the performance point (Fig. 10), which is characterised by the tsunami lateral force at the considered inundation depth. As previously mentioned, such a point is the only one where the assumed lateral force distribution is consistent with the actual base shear. The comparison amongst the different load discretisations is limited to the performance point of each CHPO analysis. The actual base shear is assessed assuming a Froude number equal to 0.60 for the different inundation depths. Such a Froude number is representative of observed tsunami onshore flows (Fig. 6). Its selection does not influence the conclusions of this section. Pushover curves with the load discretisations (A) and (C) exhibit similar trends, whereas different behaviour is observed for the load discretisations (B) and (B*). However, the tsunami force for (B) is lower than the resulting force of the load distribution, since the force acting in the first half-interstorey height is not considered. Despite this, the top displacement demand at the performance point for the load discretisation (B) is similar to the corresponding demands for (A) and (C) (Fig. 10), whilst (B*) exhibits a much larger displacement demand. It is finally noted that the structure exhibits collapse for the load discretisation (B*) in case a 19 m inundation depth is assumed. In such a case the tsunami peak force exceeds the maximum base shear.

The comparison is performed at different inundation depth levels; the predicted IDR at the first storey and the shear force in column 1011 (Fig. 2) are compared to their corresponding reference values (Fig. 11), estimated with the load discretisation (A)

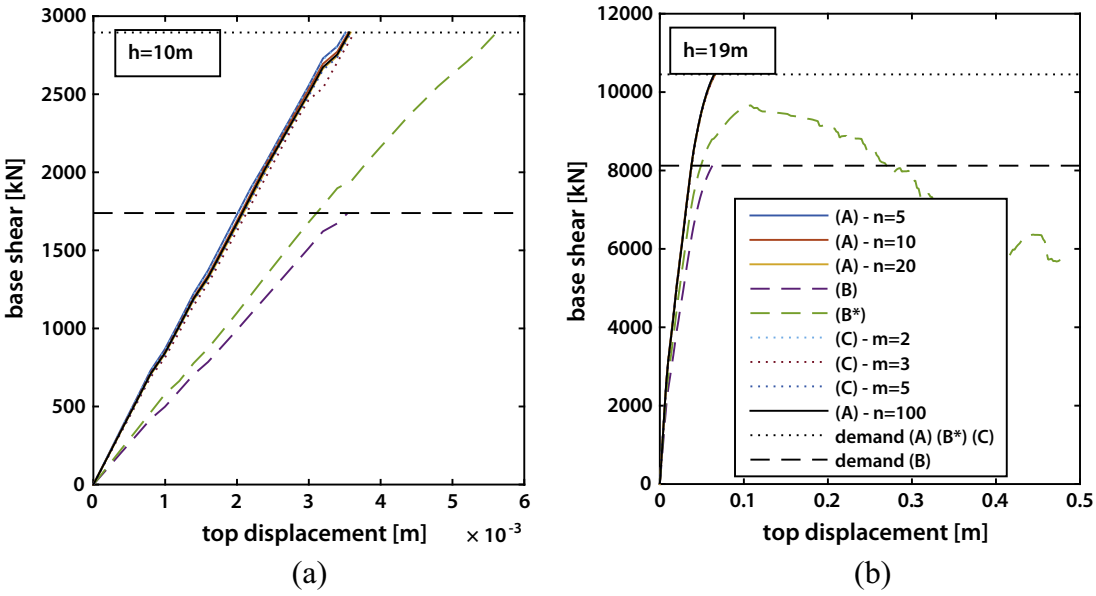

Fig. 10. Tsunami pushover curves up to the tsunami peak force for (a) 10 m and (b) 19 m inundation depths. Note that the two graphs are characterised by different scales in order to facilitate their interpretations.

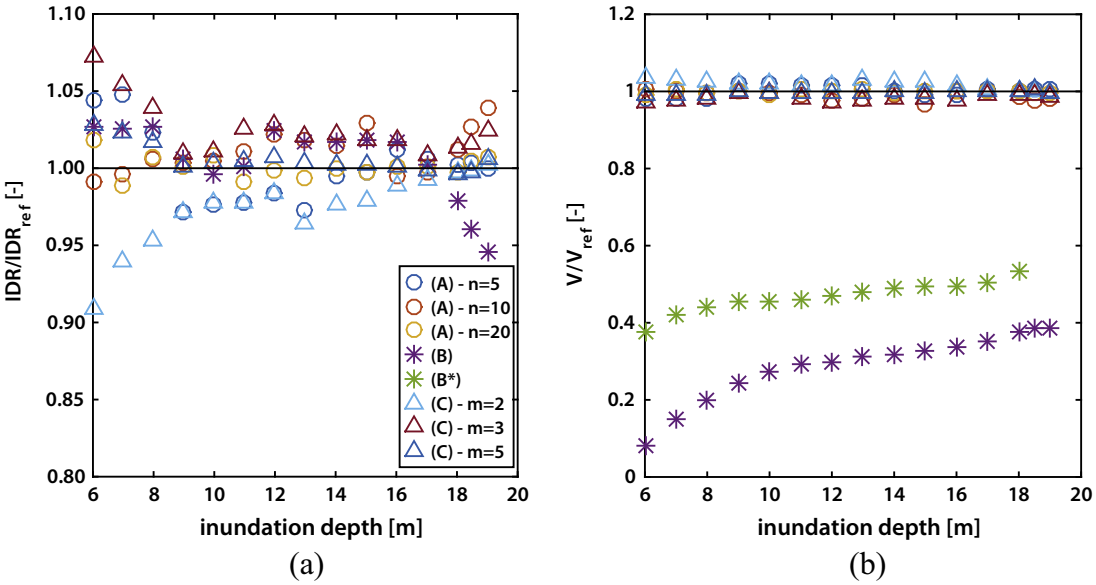

Fig. 11. Overestimation of (a) IDR at the first floor and (B) shear demand in column 1011 due to different load discretisations. Note that IDR ratios for the load discretisation (B*) are much larger than 1.1 and are not shown in the plot.

and $n = 100$. It is confirmed that the load discretisation (B*) leads to an overestimation of IDR (note that in Fig. 11a the ratios typically exceed 2.0); the load discretisation (B) exhibits an error in the range of about 5%, either safe- or unsafe-sided, for low-to-moderate displacement demands; instead, it might underestimate IDR by more than 15% when the structure is close to collapse. Both (B) and (B*) show a significant underestimation of the shear in column 1011; such an underestimation is in the range 60–85% for the load discretisation (B). The load discretisations (A) and (C) lead to an error which is typically smaller than 5% both in predicting IDR and shear. The load discretisation (C) with $m = 5$ is characterised by the greater accuracy among the selected load discretisation (C). It is interesting to note that smaller n values might induce either an underestimation or an overestimation of the demand.

The load discretisation (A) is not suitable when a VHPO is employed, since the load application point would not be constant for a variable-height load pattern. In view of the above discussion, all further analyses presented in this paper are performed using the load discretisation (B) and the load discretisation (C) with $m = 5$. Although the load discretisation B does not yield good results, it is taken forwards to the fragility analysis as it has been adopted in the past tsunami studies [9,39].

4. Tsunami pushover methods

The different nonlinear static pushover methods are first compared to each other in terms of their abilities to predict the response of the structure under tsunami actions. Then, the time-history analysis results are presented and compared with those resulting from the pushover methods. Observations are made as to the advantages and limitations of the pushover methods in reproducing the building response observed in the time-history analysis.

The different pushover methods are used to evaluate the response of the reference structure to a given tsunami action. This comparison considers both load discretisations (B) and (C) with $m = 5$ in the latter case. Both triangular and trapezoidal load patterns are considered, as well as the two different blocking ratios. For ease of understanding, it is preferred to first present the results for the 0.1 blocking ratio and the triangular load pattern. The results related to different blocking ratios and load patterns are commented on at the end of the section.

For a given combination of load pattern – load discretisation – blocking ratio, a single VHPO is executed, whereas multiple CHPOs are performed assuming different inundation depths. The comparison is performed considering $Fr = 0.60$. A performance point can be estimated for each CHPO as the demand point characterised by the force corresponding to $Fr = 0.60$. An equivalent VHPO is estimated from the CHPOs and compared to the VHPO curve (Fig. 12). A particular care is taken in defining different discrete tsunami loads, which reflect both the assumed inundation depth and force amplitude time-histories. For instance, a load at a given storey is set to zero until the inundation depth exceeds that storey height. It should be recalled that the VHPO analysis is not suitable to investigate the post-peak behaviour when the structure exhibits a softening behaviour. The analysis fails to converge as the peak building strength is reached as it is evaluated by a load-control integrator. However, VHPO is considered to be a more refined analysis compared to CHPO, given its more realistic implementation of a time-dependent tsunami load. VHPO is therefore treated as the reference analysis. The bias induced by the CHPO analysis, which is favoured in the existing literature, is estimated.

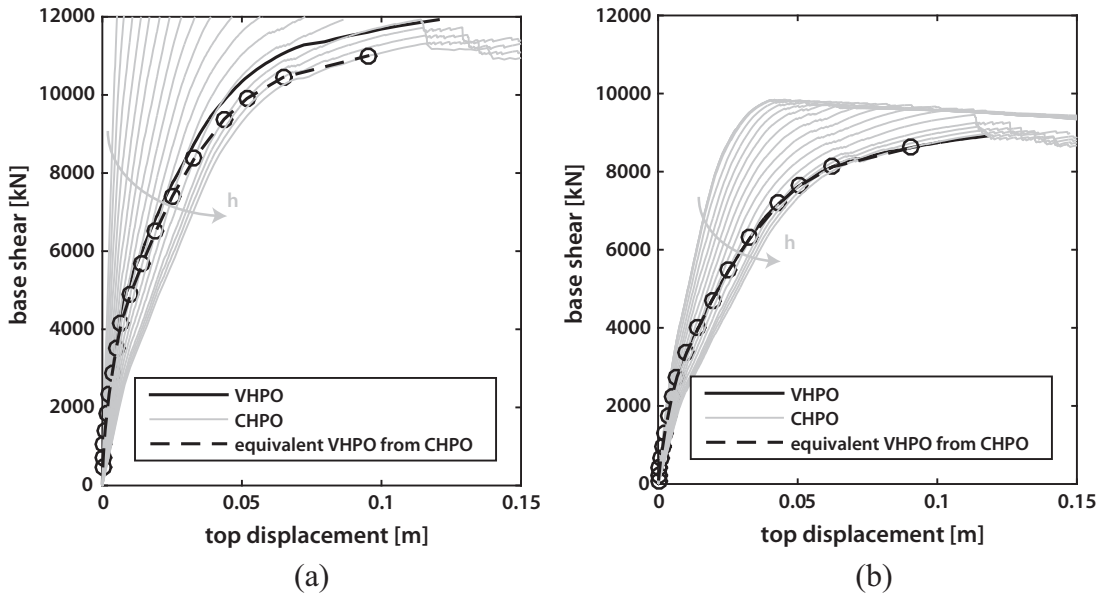

Fig. 12. Variable height pushover analysis (VHPO) versus constant height pushover analysis (CHPO): pushover curves for (a) load discretisation C and (b) load discretisation B. Note that performance points in CHPO are highlighted with black circles.

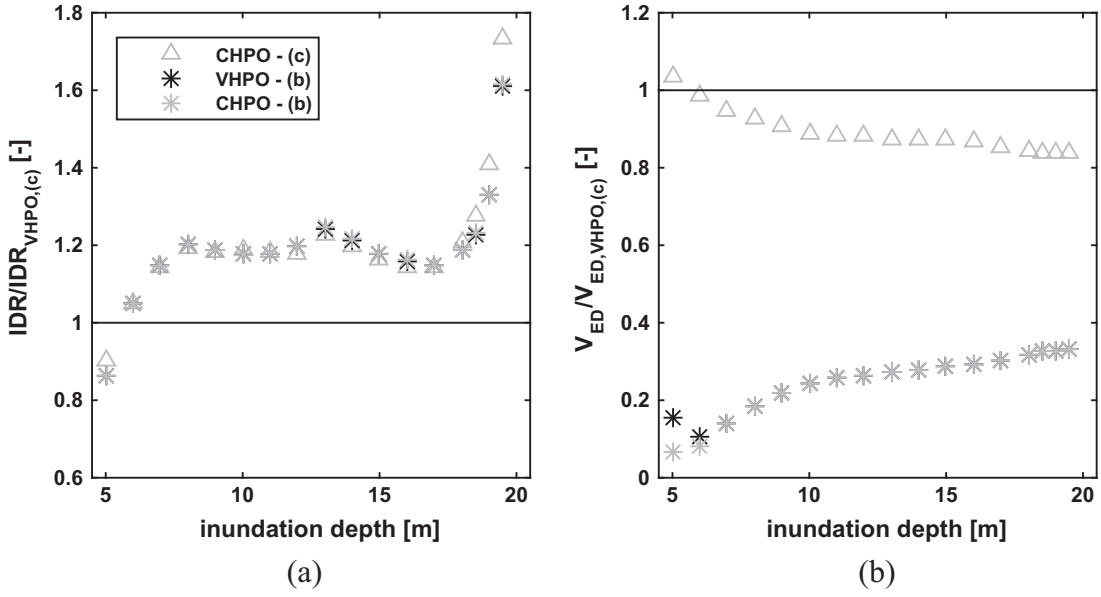

Fig. 13. Overestimation of (a) IDR at the first floor and (b) shear demand in column 1011 due to analysis method.

Comparison of the CHPO and VHPO pushover curves shows that they match well for the load discretisation (B), whereas a noticeable mismatch is observed for the load discretisation (C). In particular, CHPO underestimates the peak strength compared to VHPO for the load discretisation (C). This phenomenon can be attributed to the different loading history subjected to column 1011 in the two considered analyses. It is observed that in this column the local nonlinear deformation due to the distributed lateral loading starts to accumulate at an earlier stage in VHPO than in CHPO. The accumulation of the local nonlinear deformation in column 1011 leads to a more effective restraint provided by the beams at the first storey level in the VHPO case. A more effective restraint causes a larger moment at the top of the column and a smaller shear span ratio at the column base. The peak force, which occurs at the activation of the plastic hinge at the column base, is therefore larger in VHPO as a result of the smaller shear span ratio. This phenomenon is not observed when the tsunami forces are applied at storey levels, i.e. for load discretisation (B), resulting in the good agreement of the results of CHPO and VHPO.

The accumulation of local nonlinear deformations in VHPO also increases the stiffness of the structure, as they tend to reduce IDR at the first storey. As a result, top displacement and IDR are overestimated by CHPO, whereas shear can be underestimated (Fig. 13). Discrepancies in IDR are significant particularly close to collapse, due to the different strengths predicted by the two analysis methodologies.

It is important to underline that the shear in column 1011 might be underestimated by more than 70% when the load discretisation (B) is adopted (Fig. 13b). Shear failure might be not detected in case tsunami load is applied only at storey levels. This is an important consideration as applying tsunami loads at storey levels is common in the existing literature [9,39].

It is also interesting to note that all CHPOs for the load discretisation (B) tend to result in the same force response value for large displacements (Fig. 12b), whereas large discrepancies are observed for small displacements. This results from the dominance of a common failure mechanism at large displacements, i.e. the failure of the ground storey and the associated base shear. Indeed, for such

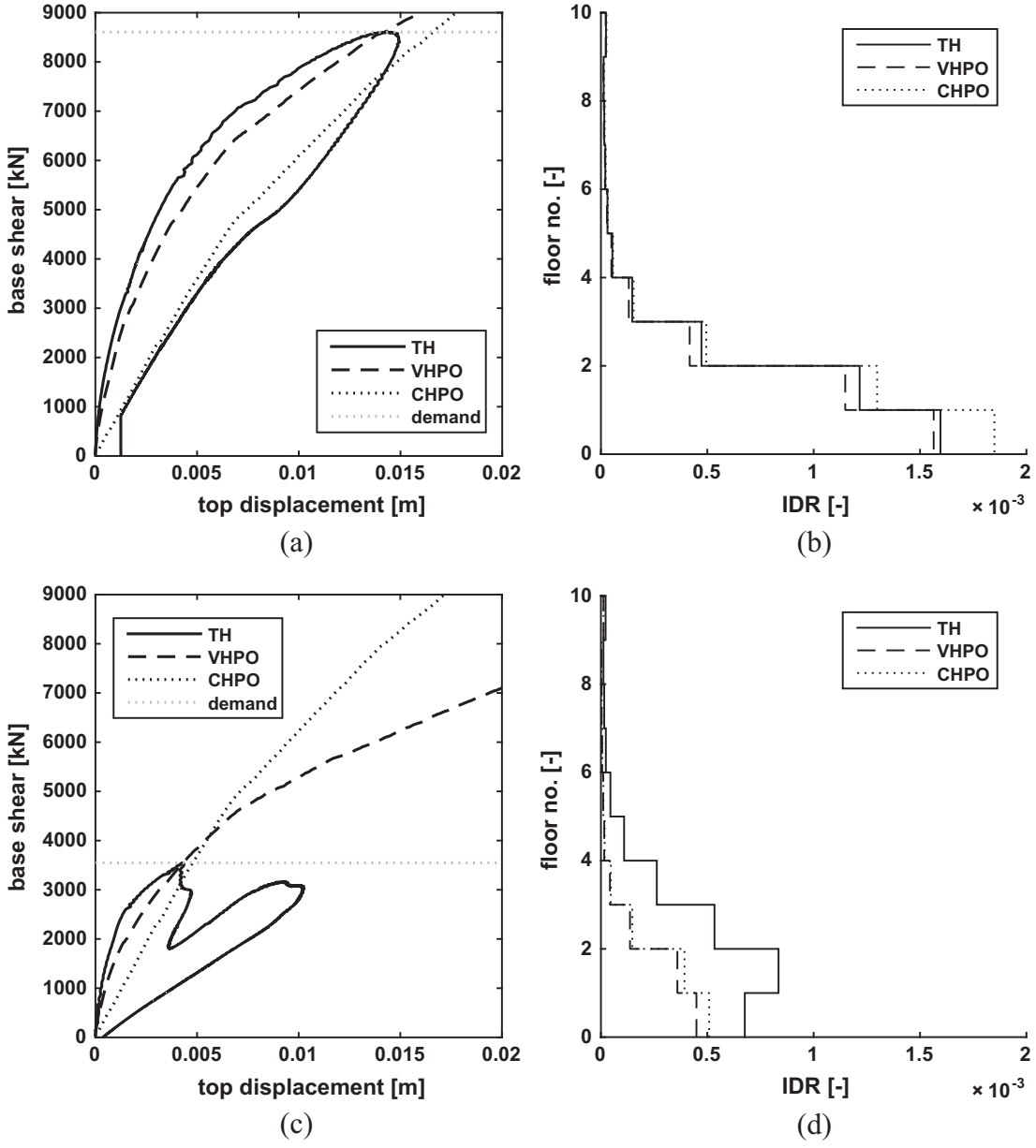

Fig. 14. Time-history vs pushover analyses for two different tsunami wave traces: (a) and (c) force-displacement envelope; (b) and (d) maximum interstorey drift demand.

a mechanism, the base shear is near constant, as it is determined by the sum of the column base resisting moments. This phenomenon is valid only for the load discretisation (B).

Similar conclusions are applicable to the 0.6 blocking ratio and for the trapezoidal tsunami load pattern. The most significant difference is that the maximum inundation depth is much lower when the 0.6 blocking ratio is adopted.

5. Tsunami time-history analysis

A question arises as to whether pushover methods can reliably estimate the demand of a given tsunami onshore inundation on the structure. Time-history analyses are therefore used as a reference, as they are able to take into account realistic flow traces and to capture any structural dynamic effects. This section focuses on the comparison of the time-history analysis with the pushover methods, in terms of demand on the structure under the tsunami inundation flow, whereas Section 6 deals with their comparison in terms of fragility curves. To illustrate the results, the outcomes of the analyses assuming a 0.6 blocking ratio are presented. It is noted that similar observations to those presented below are also seen in the case of the 0.1 blocking ratio. However, as the 0.1 blocking ratio leads to smaller forces compared to the 0.6 blocking ratio, none of the analyses for the 0.1 blocking ratio cause collapse. All the analyses are performed with the load discretisation (C).

The TH analysis is performed by applying 249 tsunami flow time-histories to the case study structure. The response of the structure is assessed by means of CHPO and VHPO for each tsunami inundation trace. The CHPO analysis is performed using the inundation height that occurs at the time step characterised by the peak force of the tsunami wave trace. The same approach is followed to assess the Froude number for the assessment of trapezoidal load pattern features (Fig. 4). The VHPO analysis assumes that the Froude number equals the value at the peak force time step of the inundation time-history. The structural demand is recorded for each of the 249 tsunami flow traces, characterised by a tsunami IM. This procedure allows the investigation of the behaviour of the structure at different tsunami intensity levels. It is similar to a "cloud" analysis, which is widely used in earthquake engineering [40] to investigate the trend of structural demand at different earthquake intensity levels.

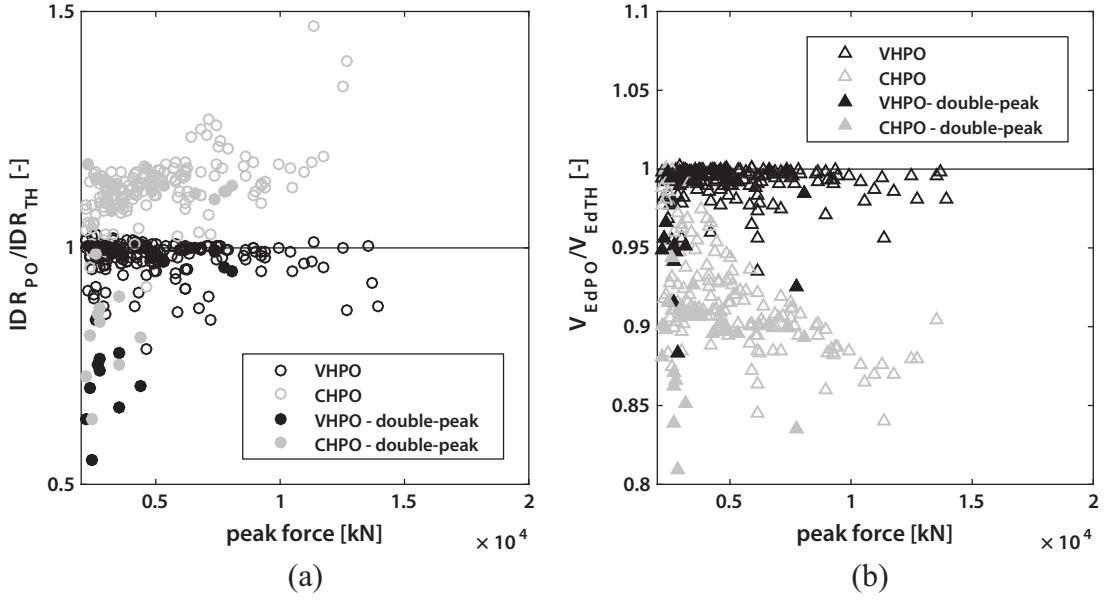

Fig. 15. Estimation of the bias induced by nonlinear static analyses for (a) IDR and (b) shear demand in column 1011, for the triangular load pattern. Double-peak wave cases are highlighted with filled markers.

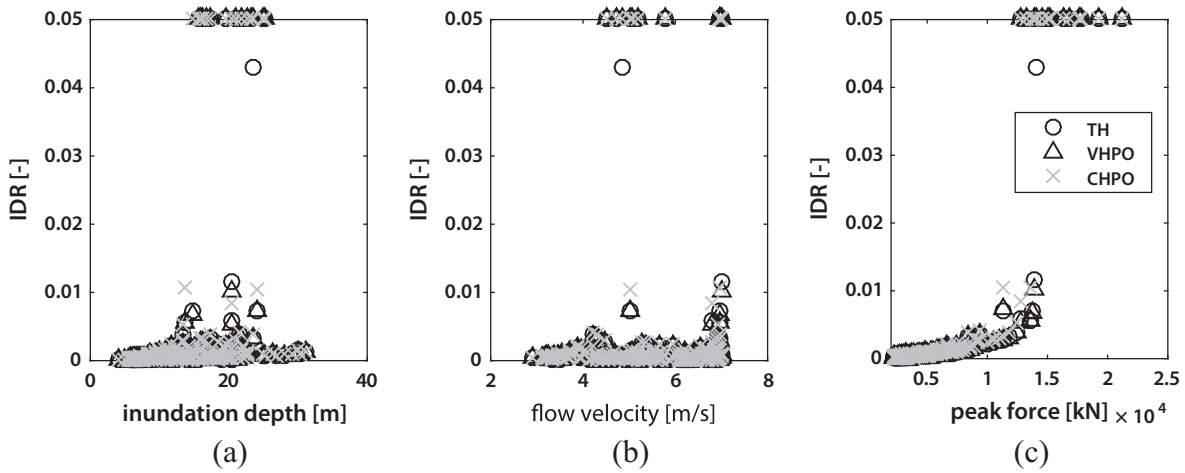

Fig. 16. Maximum IDR trend vs different tsunami IMs, assuming a triangular load pattern: (a) inundation depth, (b) flow velocity and (c) peak force.

Assessment of the structural demand is straightforward in the TH analysis, whereas it is estimated at the performance point for the pushover analyses. It is worth recalling that the performance point is characterised by the intersection of the pushover curve with a base shear equal to the peak force of the considered tsunami wave trace (Fig. 14). If the latter exceeds the peak strength of the structure predicted by the pushover analysis, the structure is assumed to have collapsed. However, collapse points are not considered in this comparison, as only the TH analysis is capable of investigating the post-peak behaviour. The comparison of analyses methods for collapse is therefore performed in terms of the ability of the methodologies to predict collapse, rather than a specific engineering demand parameter.

Overall, up to the collapse level, it is observed that the pushover methods give a good prediction of the structural demand when compared to TH (Fig. 14a and b). CHPO tends to slightly overestimate the displacement demand, as highlighted in the previous section. However, in a few cases a large discrepancy between TH and pushover methods is observed (e.g. Fig. 14c and d). The occurrence of these cases corresponds to the situations when the tsunami inundation force time-history is characterised by a double-peak, which subjects the structure to a two-cycle load. The second cycle of the time-history may induce larger displacements than the first cycle, as the structure has already sustained damage due to the first cycle and therefore has a reduced stiffness (as seen in Fig. 14c). In total, 25 out of the 249 tsunami inundation time-histories are characterised by such a double-peak pattern. The double-peak time-histories are typically recorded at locations along the Sanriku ria coast, where wave reflection along the coastline might have caused a double-peak wave to occur. A few of the double-peak wave time-histories also occur along the Sendai coastal plain, probably due to the vicinity of the river or due to the irregularity of the land elevation. These are included in the following analysis but their results are highlighted.

Comparison of the three considered analysis methodologies can be performed in terms of normalised demand quantities (Fig. 15). The demand is assessed in terms of both base shear in column 1011 and maximum IDR at the ground storey, and the structural response predicted by the pushover methods is normalised with respect to that from the TH analysis. Fig. 15 shows that VHPO provides a good estimate of both the shear and IDR for a wide range of tsunami time-histories. In several cases, VHPO may induce an underestimation of IDR due to the above-mentioned double-peak in tsunami force time-history, i.e. up to 50% underestimation for low tsunami force applied in the first cycle/peak. It is noted that as the applied tsunami force of the first cycle/peak increases, the discrepancy between VHPO and TH diminishes since the structure is already subjected to large nonlinearity by the time the second cycle is applied. It is observed that CHPO results in a worse prediction of the structure response with respect to TH as compared to VHPO. It overestimates IDR and underestimates shear in column 1011 by 5–20% in both cases. A significant overestimation of IDR is exhibited close to collapse, which can be explained by the lower peak force and the pushover curve shape of CHPOs (Fig. 12a). In both cases of VHPO and CHPO, the double-peak traces result in the largest discrepancies in the IDR prediction, but do not affect the dispersion of results for the base shear, as would be expected.

6. Fragility assessment: comparison among different analysis methodologies

This section compares the different analysis methods in terms of their abilities to predict collapse. This is done by comparing the collapse fragility curves for each analysis method, considering global structure collapse as defined in Section 2.6 and local shear failure mechanisms. It is postulated that identification of potential biases in the estimation of fragility curves helps the interpretation of differences among the considered analysis methodologies. For this comparison, different tsunami IMs are used to represent the tsunami inundation flow. Only the results of the analyses using the 0.6 blocking ratio are considered here, since a global failure is never detected for the 0.1 blocking ratio.

Fig. 16 shows the maximum IDR obtained for each methodology versus different tsunami IMs. The aim of the first analysis is to understand which tsunami IM is best suited to represent the structural analysis data in a fragility assessment. The maximum IDR is selected as it is representative of the demand on structural and (some) non-structural elements, and is conventionally used in earthquake engineering to determine structural damage [41]. For clarity of the illustration, it should be noted that in Fig. 16 all pushover analyses showing global failure are assigned with an IDR of >0.05 in the plots; this is because all TH analyses exhibiting IDR larger than 0.05 exhibit global failure according to the "20% decay" criterion presented in Section 2.6. Tsunami IMs that have been adopted in the literature for empirical tsunami fragility functions are considered herein, namely, maximum inundation depth, maximum flow velocity, and peak force. The first two IMs can be assessed directly from the tsunami inundation traces, whereas the peak force is assessed according to the procedure presented in Section 2.3.

The IM-IDR trends show that the peak force is better correlated to IDR than the flow velocity and inundation depth (as expected). IDR values are seen to increase up to a peak force range of 12,000–15,000 kN, where some analyses denote collapse and others do not. Much more scattered responses are predicted by the other IMs. It can be therefore concluded that the tsunami peak force is the most efficient IM among the ones considered in this study. The inundation depth is not an efficient IM despite the force distribution being significantly influenced by it. The peak force is an efficient IM since failure occurs as soon as it exceeds the structural strength and the structural strength is not significantly influenced by specific features of the tsunami wave trace. Indeed, either 1-storey or 2-storey local mechanism leads to the failure of the structure for all considered tsunami wave traces and the structural

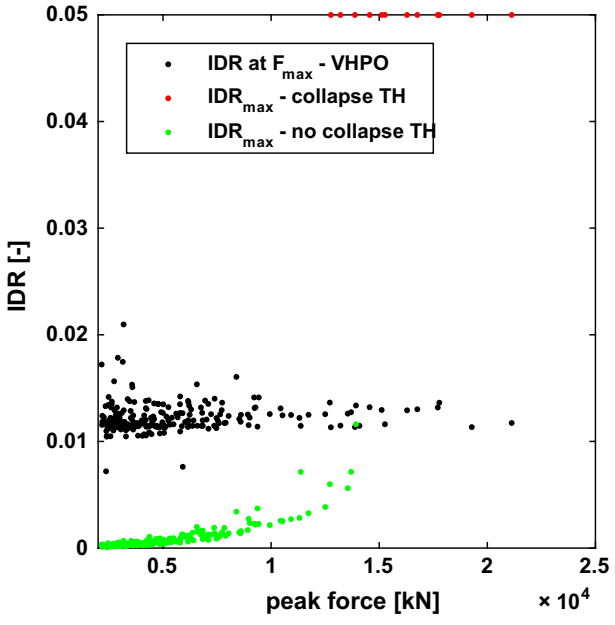

Fig. 17. IDR for TH analysis compared to the IDR occurring at maximum force in VHPO considering triangular loads.

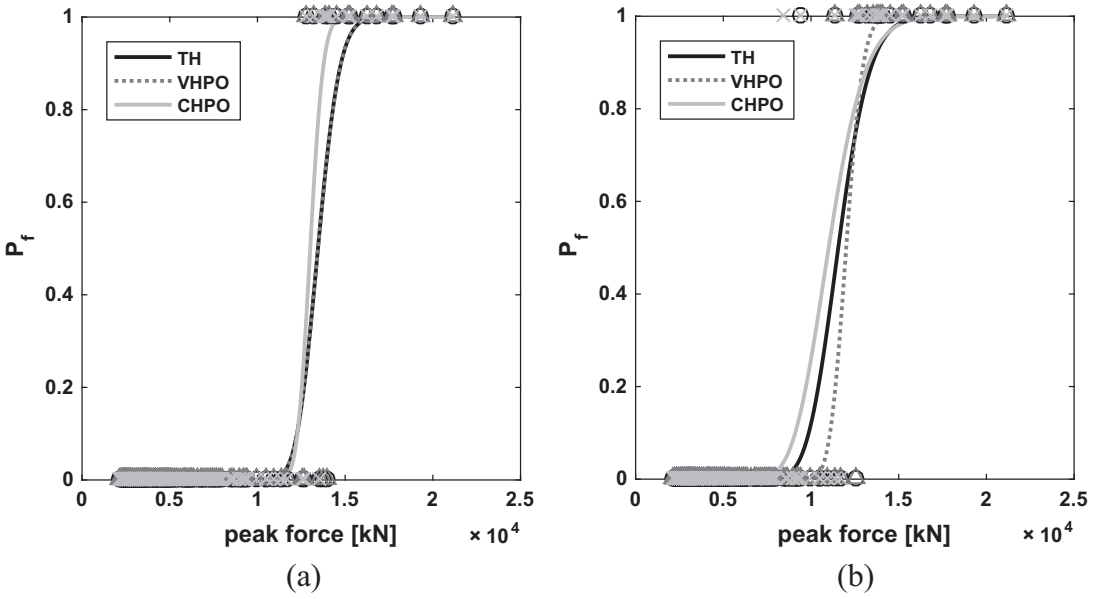

Fig. 18. Fragility curves for the global failure limit state considering (a) triangular loads and (b) trapezoidal loads.

strength associated with these mechanisms is included in a narrow range of base shear.

It is interesting to note that for the TH analysis results there is a jump in response between IDR equal to 0.015 and 0.050 in Fig. 16. This indicates the sudden failure of the structure under tsunami actions for the TH analysis. As the tsunami force exceeds the structural strength, any increase in force is absorbed by inertia and damping forces. Such forces lead the structure to large displacements abruptly. The PO analyses are able to define demand points only in the pre-peak region, which is characterised by IDR smaller than 0.015. However, given the sudden nature of collapse observed in the TH post-peak, the collapse criteria assumed for the PO analyses (i.e. collapse occurs when the tsunami force exceeds the structure peak PO response) may be considered as adequate. This conclusion is strengthened when the second definition of the global collapse adopted is examined, i.e. where collapse in the TH analysis is identified at the attainment of an IDR equal to the one occurring at the maximum force value in the PO analyses (Section 2.6). Such a collapse criterion is defined in order to use similar criteria for both TH and PO methods. The maximum demand in terms of IDR for the TH analyses is compared to the IDR occurring at the maximum force value in the corresponding PO analysis (black dots) in Fig. 17. The TH analysis results showing collapse according to the 20% decay rule are depicted in red, whereas no-collapse cases are highlighted in green[1]. It is demonstrated that this collapse criterion yields the same outcomes of the 20% decay rule. All collapse cases exhibit a demand larger than the capacity and all no-collapse cases exhibit an IDR smaller than the threshold defined according to the PO analyses. Again, this confirms that the sudden failure of the structure occurs as soon as the maximum force in the PO curve is attained.

As the two global collapse criteria for TH are essentially identical, only the 20% decay criterion is taken forwards to construct collapse fragility curves using the peak force as IM. Such curves yield the probability that the structure has exceeded the collapse limit state for a given IM. The first part of the investigations focuses on fragility curves due to global failures, neglecting the occurrence of shear failure in the elements. Their assessment is performed by

[1] For interpretation of color in Figs. 8 and 17, the reader is referred to the web version of this article.

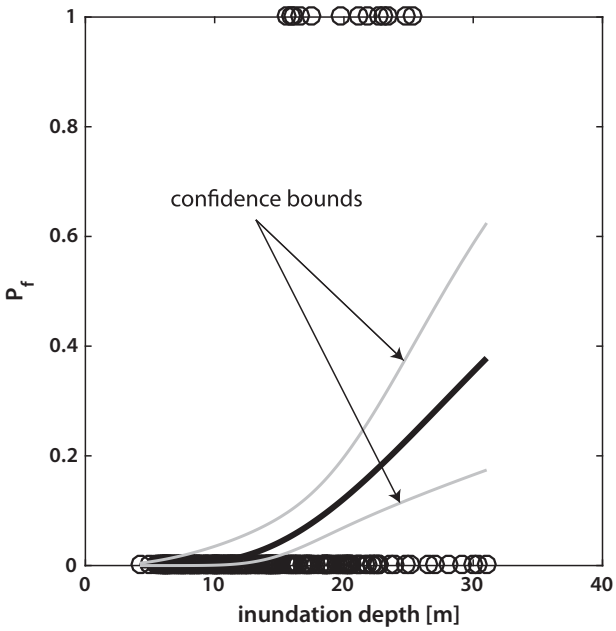

Fig. 19. Fragility curve and confidence bounds for global failure limit state for triangular loads and inundation depth as IM considering TH results.

considering the output of the analysis for each tsunami inundation time-history as a binary variable: 1 and 0 for the collapsed and non-collapsed cases, respectively. A point characterised by the tsunami peak force and the binary variable can be plotted for each analysis (Fig. 18). A logistic regression with a probit link of the data points is employed [42]. The natural logarithms of the data are used in order to obtain a lognormal fragility curve. The process is repeated for the three different analysis methodologies and for the two considered load patterns and then the bias induced by the pushover methods is estimated in comparison to TH.

Fig. 18 presents the fragility functions obtained for the three methodologies. In these plots, VHPO is seen to provide a fragility function that closely matches the TH method in the case where the triangular load pattern is adopted. A larger discrepancy of the

fragility curves is noticed for the trapezoidal load pattern. Such an agreement is achieved despite the different collapse identification methods adopted for the two analyses (Section 2.6). It confirms that when the peak force of the structure is achieved, the failure is sudden. Hence, the bias due to the adoption of pushover analysis is very limited in case a VHPO is performed. The mean collapse fragility curves of the CHPO methods are slightly shifted with respect to the TH curves, showing a higher fragility. The systematic underestimation of the peak force discussed in Section 4 is the main cause of this phenomenon. However, the fragility function shows that CHPO provides a conservative structural assessment methodology. The use of the trapezoidal loads leads to an even larger fragility. This can be explained by the lever arm, which is larger with the trapezoidal loads than with the triangular load distributions.

Empirical fragility functions are typically developed using the peak inundation depth as IM. For this reason, Fig. 19 presents the fragility functions obtained using peak inundation depth as IM. It is observed that the logarithmic dispersion β of this fragility curve (0.51), is much larger than that observed in the fragility curves developed with the peak force as IM (Fig. 19), which confirms the worse efficiency of the inundation depth as IM than the peak force.

The collapse of structures may be caused by the occurrence of shear failure in key structural elements. In particular, for the adopted structure and load patterns, the shear failure in column 1011 (i.e. 1st storey column where tsunami loads are applied; Fig. 2) is always observed to anticipate the failure of the structure. Shear safety factors can be estimated for each tsunami inundation time-history according to the different analysis methodologies (Fig. 20a and b). The fragility curves can then be re-derived considering local shear failure in addition to global failure for the two different load patterns (Fig. 20c and d).

VHPO again is seen to provide a close match to the mean collapse fragility curve assessed with TH. Instead, CHPO predicts a lower fragility as a consequence of the shear demand underestimation previously identified (i.e. see Fig. 15). From a design perspec-

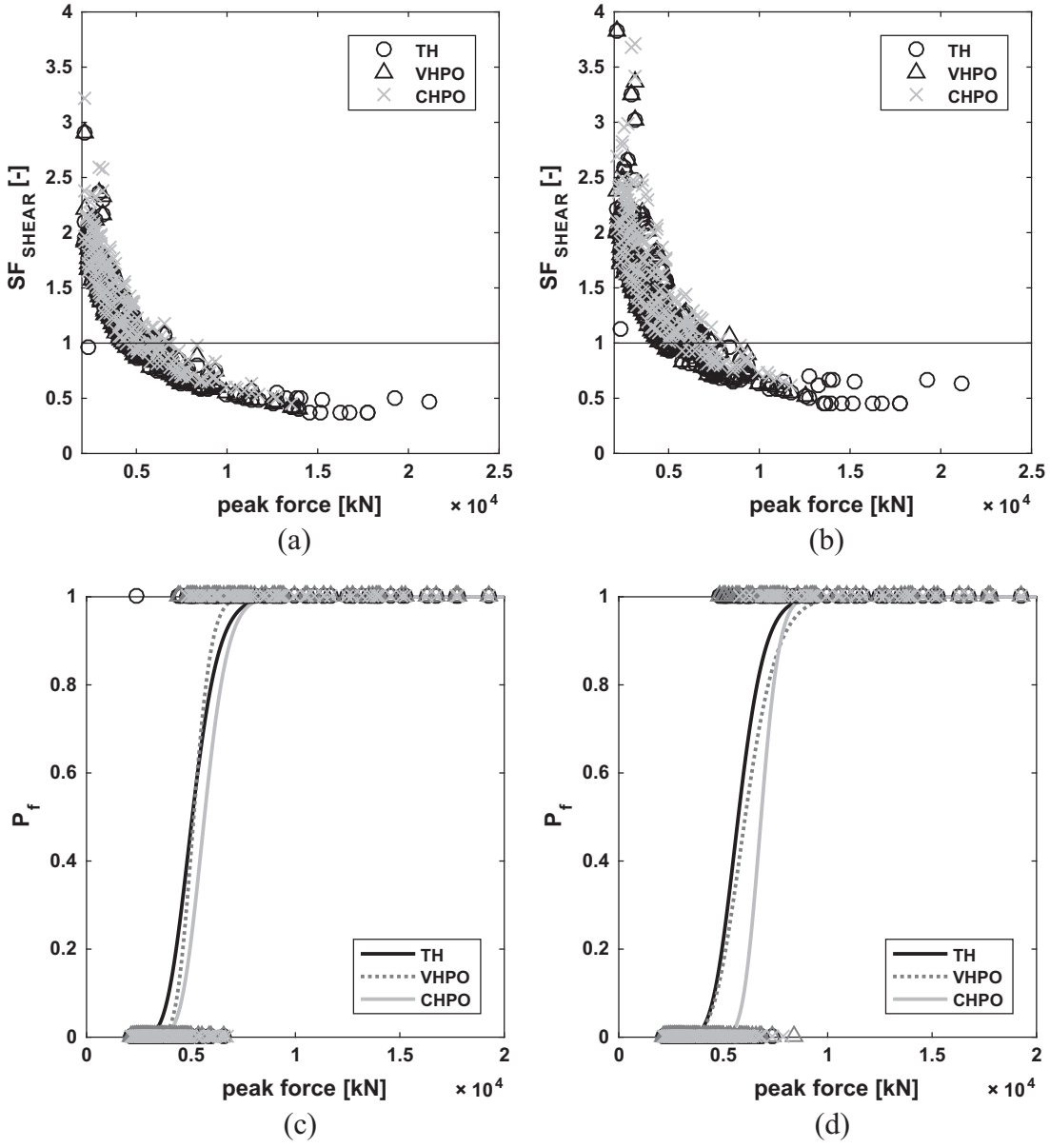

Fig. 20. Shear safety factor in terms of shear demand in column 1011 for (a) triangular and (b) trapezoidal loads; fragility curves considering shear failure for (c) triangular and (d) trapezoidal loads.

Table 3
Fragility curve parameters for global and local failures.

		Triangular loads		Trapezoidal loads	
Failure mode	Analysis	x_m [kN]	β	x_m [kN]	β
Global	TH	13,450	0.073	11,553	0.123
	VHPO	13,450	0.073	12,006	0.062
	CHPO	13,008	0.045	11,007	0.149
Local	TH	5062	0.196	5720	0.174
	VHPO	5135	0.128	6053	0.198
	CHPO	5644	0.156	6815	0.100

tive, CHPO might give an unsafe-sided estimation of collapse fragility due to the shear failure. The use of the trapezoidal loads leads to an even lower fragility prediction, contrary to the global failure case. This can be explained by smaller shear demands at the column base due to the load pattern shape. Hence, while the trapezoidal load patterns might be more demanding in terms of global failure modes, the triangular load patterns typically induce a severer shear demand on lower storeys of the structure.

Comparison of the constructed fragility curves shown in Fig. 20c and d shows that the fragility assessment is significantly influenced by local shear failures. The assessment of this particular structure that has been designed to resist earthquakes and tsunamis to modern Japanese codes suggests that this design code underestimates the shear demand on columns due to tsunami. Moreover, the dispersion in the collapse assessment, denoted by the logarithmic standard deviation of the lognormal distributions, is always lower than 0.20 for the considered structure (Table 3). Such a dispersion considers only the uncertainty due to tsunami wave input. Additional uncertainties, e.g. material properties, will be considered in future studies. This confirms the good efficiency of the peak force, which is able to predict the occurrence of collapse in a structure subjected to tsunami action with relatively low uncertainty.

7. Conclusions

Current guidelines for the design and assessment of buildings under tsunami actions do not explicitly state how best to apply the tsunami loads to the building in structural analysis nor which analysis methods to use in order to assess the structural response to the tsunami loads. Despite the recognised limitations of this study (i.e. a single case study structure that is assumed impermeable, is used, that buoyancy forces and debris impact are neglected, and only triangular and trapezoidal net force distributions are assumed), this paper provides some initial guidance on both these points.

The paper presented a comparison of different nonlinear static analyses versus dynamic analyses in assessing tsunami impact on buildings. In particular, three different analysis methodologies of constant-height pushover (CHPO), variable-height pushover (VHPO), and time-history (TH) analyses were compared in terms of their abilities to predict structural response and their accuracy in assessing collapse fragility curves for tsunami actions. A reinforced concrete frame tsunami evacuation building was selected as a case study for the comparative study and was subjected to the simulated 2011 Tohoku tsunami inundation flows. A tsunami inundation simulation was employed to define a set of tsunami inundation time-histories in terms of inundation depth and flow velocity at different sites in the Tohoku region of Japan. Tsunami force was evaluated according to a recent formulation, which was modified in this study in order to be applicable to a generic tsunami inundation trace. Two different load patterns, i.e. triangular and trapezoidal, were adopted to distribute the tsunami force along the height of the structure. A load sensitivity analysis was firstly performed, aiming to assess how to discretise the tsunami loads on the modelled structure. It was demonstrated that the tsunami load should be distributed along the height of the structure with a proper discretisation scheme. Of the load discretisation trialled, type C (with five load application points per storey) was seen to provide the best solution for two main reasons. Firstly, it can be employed for analyses with variable-height load patterns, (e.g. VHPO), and secondly, it provides negligible bias in the assessed structural response. It was therefore recommended for use in the fragility analysis of structures subjected to tsunami. In the case where tsunami loads were lumped at storey levels, a significant underestimation of the shear demand was observed, whereas drift demand may be overestimated, especially in the vicinity of structural failure.

The two pushover analysis methodologies, i.e. CHPO and VHPO, were compared to the TH analysis in terms of their abilities to predict structural response for an extensive set of simulated tsunami inundation time-histories. It was found that the results of VHPO provide a good prediction of the engineering demand parameters and collapse fragility curves obtained from the TH analysis under a wide range of tsunami time-histories. CHPO resulted in a worse prediction of the demand; it overestimated the maximum interstorey drift ratio and underestimated the column shear at the ground floor by about 5–20%. It also provided a larger fragility in case global failure was considered and a smaller fragility for local (shear) failure. Such a discrepancy was about 10% in median fragility value. On the basis of these results, it can be concluded that PO methods are a good proxy for TH. In particular, it is recommended that VHPO be used in future fragility analysis of buildings subjected to tsunami. Nevertheless, the current application indicates that CHPO may be still used for fragility assessment with limited increase in uncertainty, considering that it is easier to implement. These results cast a doubt on the reliability of past analytical fragility curves/tsunami building response studies that have been carried out using CHPO or variations of this approach, i.e. [9,10].

It should be highlighted that pushover methods were found to be inadequate in cases where the tsunami inundation force time-history is characterised by a double-peak, which subjects the structure to a two-cycle load. It was also found that tsunami peak force is better correlated to the maximum interstorey drift ratio than flow velocity and inundation depth, and results in fragility curves with lower dispersion values. It was therefore suggested that future analytical fragility functions for tsunami be produced using the peak force as the intensity measure.

Acknowledgements

This work was supported by the Engineering and Physical Sciences Research Council in the framework of CRUST project (EP/M001067/1) and by the European Research Council in the framework of URBANWAVES project (ERC Starting Grant: 336084). The contributions of Prof Ian Eames to tsunami load assessment on structures and Dr. Raffaele De Risi to the tsunami simulation are gratefully acknowledged.

References

[1] Rossetto T, Peiris N, Pomonis A, Wilkinson SM, Re D, Koo R, et al. The Indian Ocean tsunami of December 26, 2004: observations in Sri Lanka and Thailand. Nat Hazard 2006;42:105–24.
[2] Kajitani Y, Chang SE, Tatano H. Economic impacts of the 2011 Tohoku-Oki earthquake and tsunami. Earthq Spectra 2013;29:S457–78.
[3] Charvet I, Ioannou I, Rossetto T, Suppasri A, Imamura F. Empirical fragility assessment of buildings affected by the 2011 Great East Japan tsunami using improved statistical models. Nat Hazard 2014;73:951–73.
[4] Suppasri A, Mas E, Charvet I, Gunasekera R, Imai K, Fukutani Y, et al. Building damage characteristics based on surveyed data and fragility curves of the 2011 Great East Japan tsunami. Nat Hazard 2012;66:319–41.
[5] Dias WPS, Yapa HD, Peiris LMN. Tsunami vulnerability functions from field surveys and Monte Carlo simulation. Civil Eng Environ Syst 2009;26:181–94.
[6] Koshimura S, Oie T, Yanagisawa H, Imamura F. Developing fragility functions for tsunami damage estimation using numerical model and post-tsunami data from Banda Aceh, Indonesia. Coastal Eng J 2009;51:243–73.
[7] Suppasri A, Koshimura S, Imamura F. Developing tsunami fragility curves based on the satellite remote sensing and the numerical modeling of the 2004 Indian Ocean tsunami in Thailand. Natural Hazards Earth Syst Sci 2011;11:173–89.
[8] Macabuag J, Lloyd T, Rossetto T. Towards the development of a method for generating analytical tsunami fragility functions. In: Second European conference on earthquake engineering and seismology, Istanbul, August 25–29 2014.
[9] Nanayakkara KIU, Dias WPS. Fragility curves for structures under tsunami loading. Nat Hazard 2016;80:471–86.
[10] Park S, van de Lindt JW, Cox D, Gupta R, Aguiniga F. Successive earthquake-tsunami analysis to develop collapse fragilities. J Earth Eng 2012;16:851–63.
[11] FEMA P646. Guidelines for design of structures for vertical evacuation from tsunamis. Redwood City, CA (US): Applied Technology Council; 2008.
[12] Latcharote P, Kai Y. Double-layer platform of high performance computing for damage prediction of RC buildings subject to earthquake and subsequent tsunami in a target area. In: Papadrakakis VP M, Plevris V, editors. COMPDYN 2015. Crete, Greece.
[13] Qi ZX, Eames I, Johnson ER. Force acting on a square cylinder fixed in a free-surface channel flow. J Fluid Mech 2014;756:716–27.
[14] Rossetto T, Allsop W, Charvet I, Robinson DI. Physical modelling of tsunami using a new pneumatic wave generator. Coast Eng 2011;58:517–27.
[15] Goda K, Yasuda T, Mori N, Mai PM. Variability of tsunami inundation footprints considering stochastic scenarios based on a single rupture model: application to the 2011 Tohoku earthquake. J Geophys Res Oceans 2015;120:4552–75.
[16] Japan Building Disaster Prevention Association. Structural design-member cross-section case studies. Minister of Land, Infrastructure and Transport specified seismic retrofitting support center. Japan Building Disaster Prevention Association; 2007 (in Japanese).
[17] Yeh H, Barbosa A, Mason BH. Tsunamis effects in man-made environment. In: Meyers AR, editor. Encyclopedia of complexity and systems science. Berlin, Heidelberg: Springer, Berlin Heidelberg; 2014. p. 1–27.
[18] Mikami T, Shibayama T, Esteban M, Matsumaru R. Field survey of the 2011 Tohoku earthquake and tsunami in Miyagi and Fukushima prefectures. Coastal Eng J 2012;54:1250011.
[19] Kakinuma T, Tsujimoto G, Yasuda T, Tamada T. Trace survey of the 2011 Tohoku tsunami in the north of Miyagi prefecture and numerical simulation of bidirectional tsunamis in Utatsusaki peninsula. Coastal Eng J 2012;54:1250007.
[20] Suppasri A, Koshimura S, Imai K, Mas E, Gokon H, Muhari A, et al. Damage characteristic and field survey of the 2011 great east Japan tsunami in Miyagi prefecture. Coastal Eng J 2012;54:1250005.
[21] McKenna F, Fenves GL. OpenSees Manual, http://opensees.berkeley.edu. . Berkeley, California: Pacific Earthquake Engineering Research Center; 2013.
[22] Mander J, Priestley M, Park R. Theoretical stress-strain model for confined concrete. J Struct Eng 1988;114:1804–26.
[23] AIJ. Design guideline for earthquake resistant buildings based on ultimate strength concepts (in Japanese); 1988.
[24] Bahmanpour A, Eames I, Richardson S, Rossetto T. Computational study of the force and surface pressure on rectangular buildings in a steady free channel flow. J Fluid Mech 2016 (under review).
[25] Goto C, Ogawa Y, Shuto N, Imamura F. Numerical method of tsunami simulation with the leap-frog scheme (IUGG/IOC Time Project). Paris, France: UNESCO; 1997.
[26] Okada Y. Surface deformation due to shear and tensile faults in a half-space. Bull Seismol Soc Am 1985;75:1135–54.
[27] Tanioka Y, Satake K. Tsunami generation by horizontal displacement of ocean bottom. Geophys Res Lett 1996;23:861–4.
[28] Baba T, Takahashi N, Kaneda Y, Ando K, Matsuoka D, Kato T. Parallel Implementation of Dispersive Tsunami Wave Modeling with a Nesting Algorithm for the 2011 Tohoku Tsunami. Pure Appl Geophys 2015;172:3455–72.
[29] Oishi Y, Imamura F, Sugawara D. Near-field tsunami inundation forecast using the parallel TUNAMI-N2 model: Application to the 2011 Tohoku-Oki earthquake combined with source inversions. Geophys Res Lett 2015;42:1083–91.
[30] Sugawara D, Takahashi T, Imamura F. Sediment transport due to the 2011 Tohoku-oki tsunami at Sendai: results from numerical modeling. Mar Geol 2014;358:18–37.
[31] Satake K, Fujii Y, Harada T, Namegaya Y. Time and space distribution of coseismic slip of the 2011 Tohoku earthquake as inferred from tsunami waveform data. Bull Seismol Soc Am 2013;103:1473–92.
[32] Fritz HM, Phillips DA, Okayasu A, Shimozono T, Liu H, Mohammed F, et al. The Japan tsunami current velocity measurements from survivor videos at Kesennuma Bay using LiDAR. Geophys Res Lett 2011;2012:39.
[33] Foytong P, Ruangrassamee A, Shoji G, Hiraki Y, Ezura Y. Analysis of tsunami flow velocities during the March 2011 Tohoku, Japan, Tsunami. Earthq Spectra 2013;29:S161–81.
[34] Hayashi S, Koshimura S. The 2011 Tohoku tsunami flow velocity estimation by the aerial video analysis and numerical modeling. J Disaster Res 2013;8:561–72.
[35] FEMA 273. NEHRP guidelines for the seismic rehabilitation of buildings. Washington (DC); 1997.
[36] Foytong P, Ruangrassamee A, Lukkunaprasit P, Thanasisathit N. Behaviours of reinforced-concrete building under tsunami loading. IES J Part A: Civil Struct Eng 2015;8:101–10.
[37] Biskinis DE, Roupakias GK, Fardis MN. Degradation of shear strength of reinforced concrete members with inelastic cyclic displacements. ACI Struct J 2004;101:773–83.
[38] Panagiotakos TB, Fardis MN. Deformations of reinforced concrete members at yielding and ultimate. ACI Struct J 2001;98:135–48.
[39] Foytong P, Ruangrassamee A, Lukkunaprasit P. Correlation analysis of a reinforced-concrete building under tsunami load pattern and effect of masonry infill walls on tsunami load resistance. IES J Part A: Civil Struct Eng 2013;6:173–84.
[40] Shome N, Cornell CA, Bazzurro P, Carballo JE. Earthquakes, records, and nonlinear responses. Earthq Spectra 1998;14:469–500.
[41] Rossetto T, Gehl P, Minas S, Douglas J, Duffour P, Galasso C. FRACAS: a capacity spectrum approach for seismic fragility assessment including record-to-record variability. Eng Struct 2016. accepted.
[42] Reese S, Bradley BA, Bind J, Smart G, Power W, Sturman J. Empirical building fragilities from observed damage in the 2009 South Pacific tsunami. Earth Sci Rev 2011;107:156–73.